Table 3. Comparison of biosynthetic metabolites in EtOH or ACR-treated JHH7 and Hc cells determined by CE-TOFMS.

Biosynthetic pathways	Metabolites	KEGG	Fold change			
			EtOH-treated JHH7 vs. Hc		ACR vs. EtOH-treated JHH7	
			Mean	SEM	Mean	SEM
Nucleotide biosynthesis	AMP	C00020	2.50	0.10	0.82	0.00
	ATP	C00002	1.64	0.02	0.72	0.01
	CTP	C00063	1.84	0.11	0.74	0.05
	dATP	C00131	1.26	0.02	0.47	0.07
	dCTP	C00458	2.74	0.06	0.69	0.07
	dTTP	C00459	1.96	0.04	0.61	0.06
	GDP	C00035	2.76	0.15	0.82	0.02
	GTP	C00044	1.67	0.11	0.74	0.04
	IMP	C00130	2.33	0.11	0.71	0.08
	PRPP	C00119	0.68	0.08	0.53	0.11
	Ribulose 5-P	C00199	0.46	0.05	0.68	0.05
	UDP	C00015	2.81	0.05	0.82	0.05
	UTP	C00075	1.22	0.04	0.68	0.02
Amino acid biosynthesis	Ala	C00041	9.23	0.31	0.79	0.02
	Asp	C00049	3.23	0.08	0.77	0.01
	Glu	C00025	1.38	0.02	0.76	0.01
	Gly	C00037	0.64	0.02	0.82	0.01
	Ile	C00407	0.80	0.03	0.79	0.01
	Leu	C00123	0.73	0.03	0.78	0.02
	Lys	C00047	1.94	0.06	0.77	0.03
	Phe	C00079	0.69	0.02	0.78	0.01
	Ser	C00065	5.31	0.20	0.81	0.02
	Thr	C00188	1.94	0.07	0.77	0.00
	Trp	C00078	0.06	0.00	0.78	0.02
	Tyr	C00082	0.71	0.03	0.79	0.02
	Val	C00183	0.83	0.04	0.78	0.02
Lipid biosynthesis	3-Hydroxybutyric acid	C01089	1.58	0.03	0.82	0.03
	DHAP	C00111	0.28	0.03	0.52	0.03

doi:10.1371/journal.pone.0082860.t003

receptors (PPARs) and summarizes the effects of ACR on ATP production was generated using IPA (Figure 7B).

Discussion

The war on cancer has continued for more than 40 years, but the gains have been limited. One potential reason for this limited success that typical drug development in oncology has focused on targets that are essential for the survival of all dividing cells, leading to narrow therapeutic windows [31]. Recent advances in metabolite profiling methodologies have generated an alternative window for cancer therapy in targeting cancer metabolism [13]. ACR, a very promising drug that is currently in clinical trials for HCC treatment, has been shown to markedly prevent the recurrence of HCC [3] and selectively inhibit HCC cell growth [5]. We have previously exploited the potential target molecules of ACR that are associated with the promotion of tumor cell proliferation [5] or angiogenesis [32]. In this study, we performed metabolome analyses in JHH7 and Hc cells treated with ACR using both NMR and CE-TOFMS technologies to further understand the molecular pathways that underlie the cancer-selective growth suppressive effect of ACR. We found that ACR selectively suppressed the enhanced nucleotide synthesis and energy metabolism of HCC cells, suggesting that metabolic pathways may be important targets for ACR's anti-cancer activity. The further study of these pathways will benefit the development of more effective cancer drugs and therapies against HCC.

Generally, the metabolic patterns of JHH7 and Hc cells were almost completely opposite to each other (Figure 2), which is consistent with previous reports that cancer cells exhibit considerably different metabolic requirements than most normal differentiated cells and supports the hypothesis that cancer may be a type of metabolic disease [33]. Although the primary cause of cancer is assumed to be at the level of gene expression, metabolites can be considered to be the end products of the cellular regulatory processes that underlie malignant cell growth such as genome instability and mutability [34]. Metabolomic comparison of HCC and control liver tissues have been carried out in several animal and human studies aiming to define metabolomic biomarkers for the early detection of HCC [35,36]. In this study, the abundance

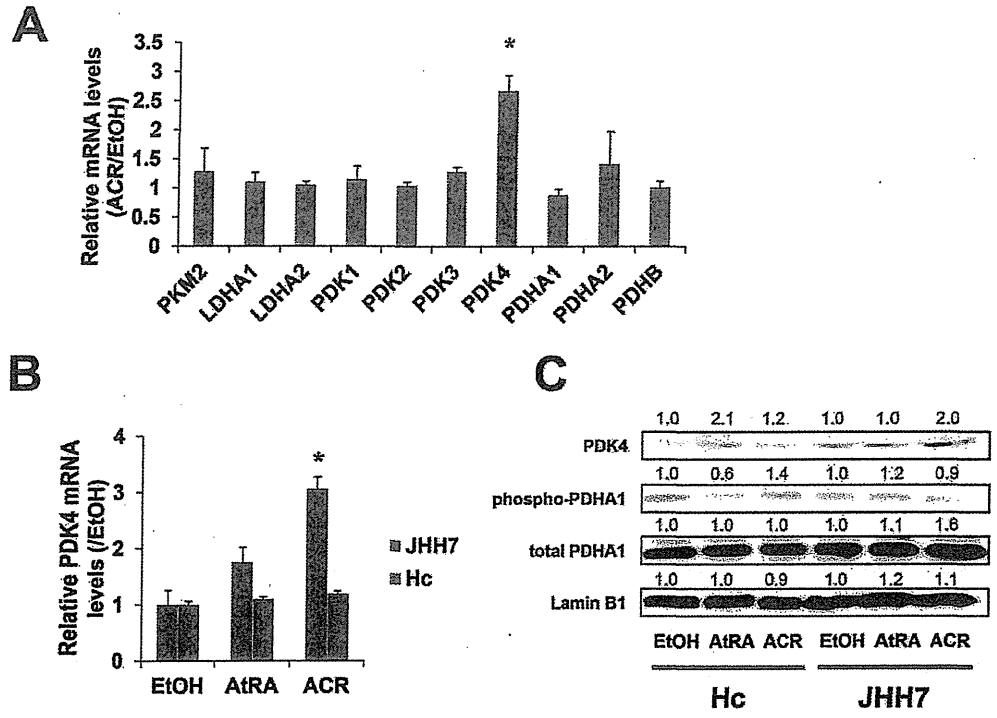

Figure 5. ACR increase the expression of PDK4 in JHH7 cells but not Hc cells. The effect of ACR on the expression of genes related to energy metabolism and ATP production in cancer cells (*A*). Levels of PDK4 mRNA (*B*) and levels of PDH4, phospho-PDHA1 and total PDHA1 protein (*C*) in JHH7 and Hc cells treated with EtOH, AtRA and ACR. The statistical significance of difference was evaluated using the Student's *t*-test.
doi:10.1371/journal.pone.0082860.g005

of 71 metabolites was found to be significantly different between JHH7 and Hc cells; 49 of these metabolites were significantly down-regulated by ACR in JHH7 cells (Figure 2 and Table S2). It is not unexpected that an IPA analysis revealed that most of these metabolites are involved in the amino acids and nucleotide biosynthetic pathways, such as "tRNA Charging", "Purine Nucleotides De Novo Biosynthesis II" and "Pyrimidine Ribonucleotides De Novo Biosynthesis" (Tables 2 and 3). It is well known that cancer cell metabolism must provide a large increase in lipid, protein, and nucleotide synthesis (biomass) to support their uncontrolled high rate of cell growth and proliferation [13]. Our findings indicate that ACR may exert its anti-cancer effect by blocking the biosynthetic processes of cancer cells. Interestingly, a bioinformatics-based anticancer drug screening program in Japan revealed that ACR shares similar anticancer activity pattern with the antipyrimidine drugs doxifluridine and cytarabine and an antipurine drug, 6-mercaptopurine, as assayed by growth inhibition against a panel of 39 human cancer cell lines (JFC39) [37,38,39].

ATP is the main energy source for the majority of cellular functions, and impaired cellular energy metabolism is the defining characteristic of nearly all cancers regardless of cellular or tissue

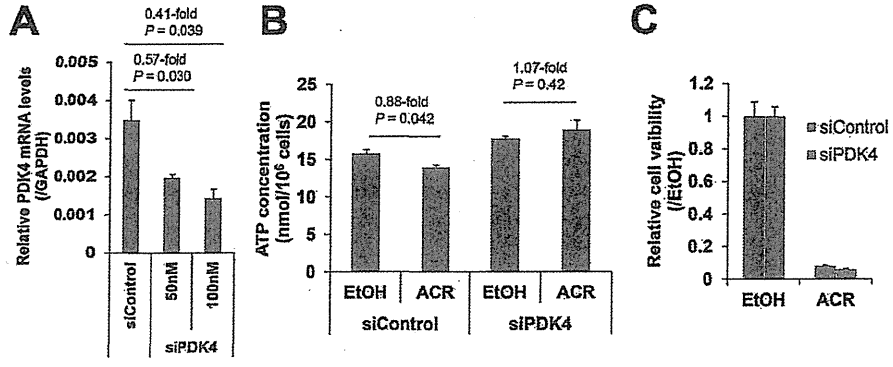

Figure 6. Functional analysis of PDK4 in JHH7 cells. The effect of siPDK4 on PDK4 gene expression (*A*). The effect of 50 nM siPDK4 on the ACR-mediated cellular ATP levels (*B*) and the proliferation (*C*) of JHH7 cells.
doi:10.1371/journal.pone.0082860.g006

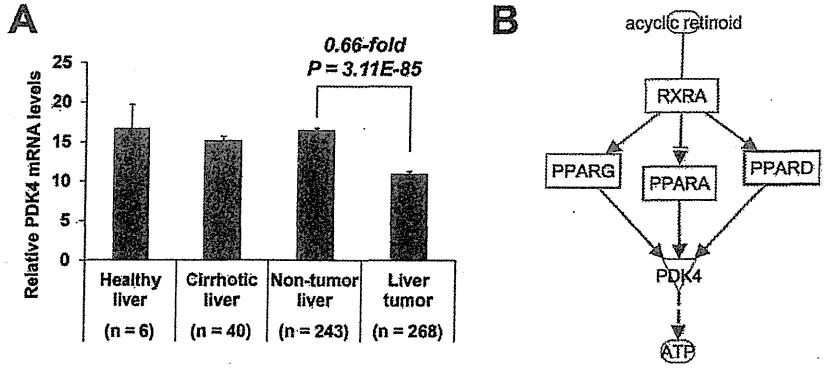

Figure 7. Clinical expression levels of PDK4. The expression of PDK4 mRNA in human liver cancer (GEO data set GSE25097) (*A*). Statistical significance was evaluated using the Mann-Whitney U test. A schematic model of the PDK4-denpendent regulatory network of ACR on ATP production in JHH7 cells generated using IPA (*B*).
doi:10.1371/journal.pone.0082860.g007

origin [33]. Of particular interest, ACR can selectively inhibit the production of ATP in JHH7 cells but not in Hc cells (Figure 4). It has been proven that chemical depletion of ATP can inhibit the growth of HCC cells [40]. This may partially explain the cancer-selective growth suppression effect of ACR. To further understand the molecular signaling mechanisms that underlie this effect, we examined the effect of ACR on the expression of energy production-related genes and observed that the expression of PDK4 was significantly enhanced by ACR in JHH7 cells but not in Hc cells (Figure 5). PDK4 is a key regulator of tricarboxylic acid (TCA) cycle; PDK4 phosphorylates and inactivates the pyruvate dehydrogenase (PDH) complex and thereby switches the energy source for the production of ATP from glucose to fatty acids. Although the cellular pyruvate level was not detected by CE-TOFMS and no effect of ACR was found on the phosphorylation of PDHA1 by western blot analysis (Figure 5C), the knockdown of PDK4 expression using RNA interference in JHH7 cells can rescue the decreased cellular ATP levels induced by ACR (Figure 6B), suggesting that PDK4 may be an important feature of ACR's anti-cancer activity. Moreover, we performed data mining using the GEO database and found that PDK4 expression is significantly down-regulated in liver tumors compared to adjacent non-tumor liver tissues (Figure 7A). The role of PDK4 in cancer therapy is complex; the inhibition of PDK4 is sufficient to inhibit the proliferation of and induce apoptosis in lung cancer cells [41], but the overexpression of PDK4 is also able to decrease ATP levels and suppress de novo lipogenesis and proliferation in breast cancer cells [30]. The specific role of PDK4 in HCC remains to be fully determined. Our results suggest that PDK4 up-regulation has a suppressive effect on HCC. Consistent with this implication, the results of IPA analysis suggest that the cancer-selective, growth-suppressive effect of ACR in inhibiting the ATP production of HCC cells may be related to a putative PDK4-dependent molecular signaling mechanism involving RXR and PPARs, as has been reported in certain fatty acid signaling pathways [42] (Figure 7B).

Although the Warburg effect is a well-recognized hallmark of cancer metabolism, it remains controversial [43]. Warburg hypothesized that tumor cells convert most of their glucose to lactate due to mitochondrial defects. However, subsequent studies showed that most tumor mitochondria are not defective in their ability to carry out oxidative phosphorylation [43]. In fact, we propose that mitochondrial oxidative phosphorylation may be important in supporting HCC cell proliferation based on the following observations: 1) the content of lactate, the major end product of glycolysis, is lower in JHH7 cells than in Hc cells (0.40-fold, Table S2) and 2) ACR up-regulates the expression of PDK4, which attenuates the flux of glycolytic carbon into mitochondrial oxidation and can reduce the production of ATP and inhibit the growth of JHH7 cells.

In summary, our study is the first to investigate the effect of ACR on cancer cell metabolism. A comparison of the metabolic effects of ACR in JHH7 and Hc cells was performed, and a JHH7-selective inhibitory effect of ACR on the production of ATP was observed. The underlying molecular signaling mechanism may relate in part to the cancer-selective enhancement of PDK4 expression, suggesting that mitochondrial oxidative phosphorylation is important in the energy metabolism of HCC cells. However, it should be noted that although PDK4 knockdown can rescue the decreased cellular ATP levels induced by ACR, no effect was observed on the inhibitory effect of ACR on the proliferation of JHH7 cells. Further research is needed to combine the cancer-selective metabolic pathways identified in this study and other signaling pathways to increase our knowledge of ACR's selective anti-cancer activity and to develop more effective cancer drugs and therapies to help us win the war against HCC.

Supporting Information

Figure S1 Statistical analysis of metabolites in JHH7 cells detected by ^{1}H-NMR. PCA score plots of the NMR spectra of JHH7 cells treated with EtOH or 10 μM ACR for 4 h and 18 h (*A*) or only 18 h (*B*).
(PPTX)

Table S1 The primers used in this study.
(XLSX)

Table S2 Quantification of major metabolites in JHH7 and Hc cells.
(XLSX)

Author Contributions

Conceived and designed the experiments: XYQ MT MS HM SK. Performed the experiments: XYQ FW. Analyzed the data: XYQ. Contributed reagents/materials/analysis tools: NI. Wrote the paper: XYQ SK.

References

1. Venook AP, Papandreou C, Furuse J, de Guevara LL (2010) The incidence and epidemiology of hepatocellular carcinoma: a global and regional perspective. Oncologist 15 Suppl 4: 5–13.
2. Llovet JM, Schwartz M, Mazzaferro V (2005) Resection and liver transplantation for hepatocellular carcinoma. Semin Liver Dis 25: 181–200.
3. Muto Y, Moriwaki H, Ninomiya M, Adachi S, Saito A, et al. (1996) Prevention of second primary tumors by an acyclic retinoid, polyprenoic acid, in patients with hepatocellular carcinoma. Hepatoma Prevention Study Group. N Engl J Med 334: 1561–1567.
4. Muto Y, Moriwaki H, Saito A (1999) Prevention of second primary tumors by an acyclic retinoid in patients with hepatocellular carcinoma. N Engl J Med 340: 1046–1047.
5. Tatsukawa H, Sano T, Fukaya Y, Ishibashi N, Watanabe M, et al. (2011) Dual induction of caspase 3- and transglutaminase-dependent apoptosis by acyclic retinoid in hepatocellular carcinoma cells. Mol Cancer 10: 4.
6. Obora A, Shiratori Y, Okuno M, Adachi S, Takano Y, et al. (2002) Synergistic induction of apoptosis by acyclic retinoid and interferon-beta in human hepatocellular carcinoma cells. Hepatology 36: 1115–1124.
7. Okada H, Honda M, Campbell JS, Sakai Y, Yamashita T, et al. (2012) Acyclic retinoid targets platelet-derived growth factor signaling in the prevention of hepatic fibrosis and hepatocellular carcinoma development. Cancer Res 72: 4459–4471.
8. Shao RX, Otsuka M, Kato N, Taniguchi H, Hoshida Y, et al. (2005) Acyclic retinoid inhibits human hepatoma cell growth by suppressing fibroblast growth factor-mediated signaling pathways. Gastroenterology 128: 86–95.
9. Kagawa M, Sano T, Ishibashi N, Hashimoto M, Okuno M, et al. (2004) An acyclic retinoid, NIK-333, inhibits N-diethylnitrosamine-induced rat hepatocarcinogenesis through suppression of TGF-alpha expression and cell proliferation. Carcinogenesis 25: 979–985.
10. Matsushima-Nishiwaki R, Okuno M, Takano Y, Kojima S, Friedman SL, et al. (2003) Molecular mechanism for growth suppression of human hepatocellular carcinoma cells by acyclic retinoid. Carcinogenesis 24: 1353–1359.
11. Suzui M, Masuda M, Lim JT, Albanese C, Pestell RG, et al. (2002) Growth inhibition of human hepatoma cells by acyclic retinoid is associated with induction of p21(CIP1) and inhibition of expression of cyclin D1. Cancer Res 62: 3997–4006.
12. Matsushima-Nishiwaki R, Okuno M, Adachi S, Sano T, Akita K, et al. (2001) Phosphorylation of retinoid X receptor alpha at serine 260 impairs its metabolism and function in human hepatocellular carcinoma. Cancer Res 61: 7675–7682.
13. Vander Heiden MG (2011) Targeting cancer metabolism: a therapeutic window opens. Nat Rev Drug Discov 10: 671–684.
14. Koppenol WH, Bounds PL, Dang CV (2011) Otto Warburg's contributions to current concepts of cancer metabolism. Nat Rev Cancer 11: 325–337.
15. Butler EB, Zhao Y, Munoz-Pinedo C, Lu J, Tan M (2013) Stalling the engine of resistance: targeting cancer metabolism to overcome therapeutic resistance. Cancer Res 73: 2709–2717.
16. El-Serag HB (2012) Epidemiology of viral hepatitis and hepatocellular carcinoma. Gastroenterology 142: 1264–1273 e1261.
17. Welzel TM, Graubard BI, Zeuzem S, El-Serag HB, Davila JA, et al. (2011) Metabolic syndrome increases the risk of primary liver cancer in the United States: a study in the SEER-Medicare database. Hepatology 54: 463–471.
18. Fujise K, Nagamori S, Hasumura S, Homma S, Sujino H, et al. (1990) Integration of hepatitis B virus DNA into cells of six established human hepatocellular carcinoma cell lines. Hepatogastroenterology 37: 457–460.
19. Qin XY, Wei F, Yoshinaga J, Yonemoto J, Tanokura M, et al. (2011) siRNA-mediated knockdown of aryl hydrocarbon receptor nuclear translocator 2 affects hypoxia-inducible factor-1 regulatory signaling and metabolism in human breast cancer cells. FEBS Lett 585: 3310–3315.
20. Wei F, Furihata K, Hu F, Miyakawa T, Tanokura M (2010) Complex mixture analysis of organic compounds in green coffee bean extract by two-dimensional NMR spectroscopy. Magn Reson Chem 48: 857–865.
21. Ohashi Y, Hirayama A, Ishikawa T, Nakamura S, Shimizu K, et al. (2008) Depiction of metabolome changes in histidine-starved Escherichia coli by CE-TOFMS. Mol Biosyst 4: 135–147.
22. Sugimoto M, Hirayama A, Robert M, Abe S, Soga T, et al. (2010) Prediction of metabolite identity from accurate mass, migration time prediction and isotopic pattern information in CE-TOFMS data. Electrophoresis 31: 2311–2318.
23. Qin XY, Akanuma H, Wei F, Nagano R, Zeng Q, et al. (2012) Effect of low-dose thalidomide on dopaminergic neuronal differentiation of human neural progenitor cells: a combined study of metabolomics and morphological analysis. Neurotoxicology 33: 1375–1380.
24. Qin XY, Kojima Y, Mizuno K, Ueoka K, Muroya K, et al. (2012) Identification of novel low-dose bisphenol a targets in human foreskin fibroblast cells derived from hypospadias patients. PLoS One 7: e36711.
25. Bronner IF, Bochdanovits Z, Rizzu P, Kamphorst W, Ravid R, et al. (2009) Comprehensive mRNA expression profiling distinguishes tauopathies and identifies shared molecular pathways. PLoS One 4: e6826.
26. Vander Heiden MG, Lunt SY, Dayton TL, Fiske BP, Israelsen WJ, et al. (2011) Metabolic pathway alterations that support cell proliferation. Cold Spring Harb Symp Quant Biol 76: 325–334.
27. Vander Heiden MG, Cantley LC, Thompson CB (2009) Understanding the Warburg effect: the metabolic requirements of cell proliferation. Science 324: 1029–1033.
28. Levine AJ, Puzio-Kuter AM (2010) The control of the metabolic switch in cancers by oncogenes and tumor suppressor genes. Science 330: 1340–1344.
29. DeBerardinis RJ, Lum JJ, Hatzivassiliou G, Thompson CB (2008) The biology of cancer: metabolic reprogramming fuels cell growth and proliferation. Cell Metab 7: 11–20.
30. Grassian AR, Metallo CM, Coloff JL, Stephanopoulos G, Brugge JS (2011) Erk regulation of pyruvate dehydrogenase flux through PDK4 modulates cell proliferation. Genes Dev 25: 1716–1733.
31. Michelakis ED, Webster L, Mackey JR (2008) Dichloroacetate (DCA) as a potential metabolic-targeting therapy for cancer. Br J Cancer 99: 989–994.
32. Komi Y, Sogabe Y, Ishibashi N, Sato Y, Moriwaki H, et al. (2010) Acyclic retinoid inhibits angiogenesis by suppressing the MAPK pathway. Lab Invest 90: 52–60.
33. Seyfried TN, Shelton LM (2010) Cancer as a metabolic disease. Nutr Metab (Lond) 7: 7.
34. Hanahan D, Weinberg RA (2011) Hallmarks of cancer: the next generation. Cell 144: 646–674.
35. Beyoglu D, Imbeaud S, Maurhofer O, Bioulac-Sage P, Zucman-Rossi J, et al. (2013) Tissue metabolomics of hepatocellular carcinoma: Tumor energy metabolism and the role of transcriptomic classification. Hepatology 58: 229–238.
36. Wang J, Zhang S, Li Z, Yang J, Huang C, et al. (2011) (1)H-NMR-based metabolomics of tumor tissue for the metabolic characterization of rat hepatocellular carcinoma formation and metastasis. Tumour Biol 32: 223–231.
37. Yamori T (2004) [Chemical evaluation by cancer cell line panel and its role in molecular target-based anticancer drug screening]. Gan To Kagaku Ryoho 31: 485–490.
38. (2004) Results of molecular target antineoplastic agents screening. Gan To Kagaku Ryoho 31 Suppl 1: 1–150.
39. Nakatsu N, Nakamura T, Yamazaki K, Sadahiro S, Makuuchi H, et al. (2007) Evaluation of action mechanisms of toxic chemicals using JFCR39, a panel of human cancer cell lines. Mol Pharmacol 72: 1171–1180.
40. Dilip A, Cheng G, Joseph J, Kunnimalaiyaan S, Kalyanaraman B, et al. (2013) Mitochondria-targeted antioxidant and glycolysis inhibition: synergistic therapy in hepatocellular carcinoma. Anticancer Drugs.
41. Bonnet S, Archer SL, Allalunis-Turner J, Haromy A, Beaulieu C, et al. (2007) A mitochondria-K+ channel axis is suppressed in cancer and its normalization promotes apoptosis and inhibits cancer growth. Cancer Cell 11: 37–51.
42. Schoonjans K, Staels B, Auwerx J (1996) Role of the peroxisome proliferator-activated receptor (PPAR) in mediating the effects of fibrates and fatty acids on gene expression. J Lipid Res 37: 907–925.
43. Ward PS, Thompson CB (2012) Metabolic reprogramming: a cancer hallmark even warburg did not anticipate. Cancer Cell 21: 297–308.

Thermotherapy Using Magnetic Cationic Liposomes Powerfully Suppresses Prostate Cancer Bone Metastasis in a Novel Rat Model

Daichi Kobayashi,[1] Noriyasu Kawai,[1]* Shinya Sato,[2] Taku Naiki,[1] Kenji Yamada,[1] Takahiro Yasui,[1] Keiichi Tozawa,[1] Takeshi Kobayashi,[3] Satoru Takahashi,[2] and Kenjiro Kohri[1]

[1]*Department of Nephro-Urology, Nagoya City University Graduate School of Medical Sciences, Mizuho-ku, Nagoya, Japan*

[2]*Department of Experimental Pathology and Tumor Biology, Nagoya City University Graduate School of Medical Sciences, Mizuho-ku, Nagoya, Japan*

[3]*College of Bioscience and Biotechnology, Chubu University, Matsumoto-cho, Kasugai, Japan*

BACKGROUND. Bone metastasis is a serious problem for individuals with prostate cancer, and the effects of the anticancer drug docetaxel (DTX) are insufficient. We therefore examined the therapeutic potential of magnetic cationic liposomes (MCL) in a novel rat model that allows the evaluation of tumor immunity. The effects of MCL thermotherapy were compared with those of DTX as a conventional therapy for the treatment of bone metastatic prostate cancer.

METHODS. Prostate tumor tissues were transplanted into the femurs of model rats divided into four groups: control, MCL, DTX, and MCL + DTX. Tumors were injected with MCL, and alternating magnetic field (AMF) irradiation was performed three times a week. Tumor proliferation and bone destruction were evaluated by proliferating cell nuclear antigen positivity, computed tomography, and CD68-positive cell number, while tumor immunity was evaluated by heat shock protein (HSP) 70 expression and CD8-positive lymphocyte number.

RESULTS. We successfully established a novel femur metastasis model of prostate cancer, and demonstrated that tumor proliferation and bone destruction in the MCL and MCL + DTX groups were significantly suppressed compared with control and DTX groups. MCL thermotherapy concurrently induced necrosis and apoptosis. The expression of HSP70 in the MCL and MCL + DTX groups was also significantly increased, and tumor immunity was enhanced through the induction of CD8-positive lymphocytes.

CONCLUSION. MCL thermotherapy was clearly more effective than DTX in treating bone metastatic prostate cancer. A combination of MCL thermotherapy and DTX therefore deserves consideration as a novel treatment for this disease. *Prostate* © 2013 Wiley Periodicals, Inc.

KEY WORDS: **magnetic cationic liposomes; bone metastasis; cell death; combination therapy; docetaxel; osteoclasts**

INTRODUCTION

Bone metastasis and lymph node metastasis are frequently observed in advanced prostate cancer [1]. Among 1,589 autopsy cases of prostate cancer patients from 1967 to 1995, 35% showed hematogenous metastases, with the most frequent involvement being bone (90%) [2–4]. Bone metastases is therefore one of the most important clinical problems faced by prostate cancer patients.

The bone microenvironment is composed of osteoblasts, osteoclasts, the mineralized bone matrix, and

Grant sponsor: Ministry of Education, Culture, Sports, Science and Technology of Japan; Grant numbers: 21592055; 21790390; Grant sponsor: Nagoya City University; Grant sponsor: Ichihara International Scholarship Foundation; Grant sponsor: Aichi Cancer Research Foundation.

No potential conflicts of interest were disclosed.

*Correspondence to: Noriyasu Kawai, Department of Nephro-Urology, Nagoya City University Graduate School of Medical Sciences, 1 Kawasumi, Mizuho-cho, Mizuho-ku, Nagoya 467-8601, Japan. E-mail: n-kawai@med.nagoya-cu.ac.jp

Received 11 October 2012; Accepted 7 December 2012
DOI 10.1002/pros.22637
Published online in Wiley Online Library (wileyonlinelibrary.com).

many other cell types. It is highly favorable for tumor invasion and growth. Crosstalk between tumor cells and the microenvironment promotes a vicious cycle of tumor growth and bone destruction [5–7], whereby metastatic prostate tumor cells in the bone microenvironment produce cytokines that stimulate osteoclastic bone resorption. This results in the release of growth factors that stimulate tumor cell proliferation from the bone matrix, such as TGF-beta [8,9], insulin-like growth factors [8], and bone morphological proteins [10]. Therefore, a different mechanism of cancer cell proliferation is observed in bone metastatic lesions compared to the primary lesion. Because excessive osteoclast activity plays a central role in the pathophysiology of bone disease at each stage of prostate cancer progression, it is necessary to suppress this activity in order to inhibit the development of bone metastatic lesions.

Highly potent inhibitors of osteoclast-mediated bone resorption such as zoledronic acid and anti-RANKL antibody are capable of suppressing osteoclast activity [11–13]; however, the antitumor activity of these agents remains unconfirmed in prostate cancer. On the other hand, anticancer drugs such as docetaxel (DTX), which has a proven effect on castration-resistant prostate cancer, inhibits the growth of cancer cells but does not suppress the activity of osteoclasts. The effects of cancer drugs on bone metastatic lesions are therefore uncertain, and the inhibition of osteoclast and tumor cell growth in the bone microenvironment can be considered important strategies for the treatment of prostate cancer bone metastases.

Thermotherapy is a promising candidate for cancer therapy that has the potential to suppress both tumor growth and osteolysis in the bone microenvironment [14]. In the clinic, heating with a radiofrequency electric field is the most common method of applying this therapy [15]; however, this may induce localized heating in tumors and unexpected hot spots in normal tissue due to the uneven distribution of electrodes. Such effects may be influenced by factors such as tumor size. In this study, we examined the efficacy of thermotherapy for prostate cancer of the bone microenvironment by using magnetic cationic liposomes (MCLs) irradiated with an alternating magnetic field (AMF) [16]. In this process, known as "MCL thermotherapy," MCLs are injected into the tumor and heated by AMF. This limits the heated area compared with conventional thermotherapy, because irradiation with AMF is carried out at the frequency at which MCLs generate heat, allowing only cancer tissue to be heated [17–19]. Using a rat model that mimics human prostate cancer bone metastasis with respect to tumor stromal interaction, we demonstrated that MCL thermotherapy concomitantly suppressed both prostate cancer cell proliferation and osteoclast osteolysis in the bone microenvironment. It was also confirmed that MCL thermotherapy simultaneously suppressed the activity of osteoclasts and the proliferation of cancer cells [16–18]. These results suggest that MCL thermotherapy may be a very useful tool for the treatment of metastases to bone lesions.

In this study, we established a novel rat metastases model of prostate cancer to evaluate tumor growth, bone destruction, and tumor immunity at the same time. This model possesses tumor–stromal interactions that mimic those of human prostate cancer bone metastasis, exhibits reduced side effects in response to repeated thermotherapy, and represents a model of a deep-site tumor compared with a previous model [16]. We also improved the MCL thermotherapy procedure in this study. First, the injection method was changed. Previously, MCLs were injected into the tumor nodule from one or two sites; however, here, we injected MCLs from four or five different sites around the tumor nodule. Second, we performed AMF irradiation at constant intervals. Previously, treatment had been stopped for 5 days after AMF irradiation because of severe exhaustion of the test rats, and this application of AMF irradiation at inconstant intervals might have been associated with an insufficient therapeutic effect in the previous study. In the present study, we were able to perform irradiation at constant intervals, thereby alleviating rat exhaustion. Finally, we increased the total MCL volume injected in order to treat a deep tumor rather than a subcutaneous tumor. We then used our rat model treated with this improved procedure to test our hypothesis that MCL thermotherapy is superior to DTX as a conventional therapy for the treatment of bone metastatic prostate cancer. In addition to evaluating the efficacy of MCL thermotherapy compared with DTX, we evaluated the effectiveness of combination therapy with both MCL thermotherapy and DTX.

MATERIALS AND METHODS

Animals

Six-week-old male F344 rats were obtained from Charles River, Japan, Inc. (Atsugi, Japan). They were randomly divided into groups of three animals per plastic cage with hard wood chips as bedding in an air-conditioned room at 22% ± 2% and 55% ± 5% humidity, with a 12-hr light/dark cycle. Food (Oriental MF; Oriental Yeast Co., Tokyo, Japan) and tap water were available ad libitum. The research was conducted according to the Guidelines for the Care and Use of Laboratory Animals of Nagoya City University Medical School, and the experimental protocol was

approved by the Institutional Animal Care and Use Committee (H21-M13).

Tumor Tissue

Androgen-independent prostate cancer tissue, PLS-P, was established in the Department of Experimental Oncology and Tumor Biology, Nagoya City University Graduate School of Medical Sciences [20]. This tumor tissue was developed from 3,2-dimethyl-4-aminobiphenyl plus testosterone-induced cancer in the dorsal prostate of male F344 rats. It forms well-differentiated adenocarcinoma with abundant connective tissue stroma, and is immunohistochemically negative for androgen receptor. This tissue can be transplanted into syngenic F344 rats [9,16,21].

Preparation of MCLs

MCLs were fabricated from colloidal magnetite (a kind gift from Toda Kogyo, Hiroshima, Japan) and a lipid mixture consisting of *N*-(a-trimethylammonioacetyl)-didodecyl-D-glutamate chloride (Sogo Pharmaceutical, Tokyo, Japan), dilauroylphosphatidylcholine, and dioleoylphosphatidyl-ethanolamine (Sigma, St. Louis, MO) in a molar ratio of 1:2:2, as described previously [22,23].

Animal Experiment

Approximately 0.5 g aliquots of PLS-P were transplanted into the femur bones of 6-week-old male F344 rats under anesthesia. An incision of approximately 1 cm was made in the skin at the femur and a pocket beneath the skin and muscle was formed using forceps. Prostate tumor tissue was then inserted into the pocket, and the incision was closed using surgical sutures and autoclips (BD Biosciences, Bedford, MA). Body weight was measured every 2 days from the start to the end of therapy. Tumor volume was also measured every 2 days from day 11 to the end of therapy. Tumor diameters were measured in three directions using an external caliper, while tumor volume was calculated using an ellipsoidal formula (tumor volume = 4/3pi(a × b × c), where a, b, and c are the 3 radii) [24,25]. One week after transplantation, autoclips were removed. Three weeks after transplantation, rats were divided into four groups (control group, MCL treatment group, DTX intravenous injection group, MCL + DTX group; number of rats per group, n = 5). The DTX and MCL + DTX groups were administered DTX (10 mg/kg) intravenously on day 0 of this experiment. MCLs (30 mg/ml) were injected directly into the tumors of the MCL and MCL + DTX groups on both the right and left sides in two separate volumes of 0.3 ml (0.6 ml in total) using a Hamilton syringe (Hamilton, Reno, NV) and a syringe pump (KDS, Tokyo, Japan). AMF irradiation was performed three times a week. On day 21 after the start of therapy, all rats were sacrificed and radiography of the transplantation sites was performed with XED-125M (Shimadzu, Tokyo, Japan) and CT (Hitachi Aloka Co. Ltd, Mitaka, Tokyo, Japan). Femur tumors with part of the femur bone were excised en bloc, fixed with 10% buffered formalin solution, and processed for histological examination. For quantitative analysis of bone destruction, the total remaining bone area in hematoxylin and eosin (H & E)-stained sections was examined under a light microscope connected to an image analysis system, including an image processor for analytical pathology (IPAP; Sumika Technos Corp., Osaka, Japan), in order to calculate the remaining bone area. Remaining bone volume was calculated by CT.

AMF Irradiation

An AMF was created using a horizontal coil (inner diameter: 7 cm; length: 7 cm) with a transistor inverter (LTG-100-05; Dai-ichi High Frequency, Tokyo, Japan) operating at 360 kHz. Magnetic field intensity was 30.6 kA/m (384 Oe). Each rat was placed inside the coil such that the tumor nodule was positioned at the center of the coil (Fig. 1A). During AML irradiation, the surface temperature of the rat at the MCL-injected tumor site was locally elevated compared with other surfaces of the rat (Fig. 1B). Temperatures at the center of the tumor and inside the rectum during application of the AMF were measured by an optical fiber probe (FX-9020; Anritsu Meter, Tokyo, Japan) inserted into the tumor and rectum. The temperature at the center of the tumor was maintained at approximately 48–49°C by controlling magnetic field intensity. The temperature at the tumor surface was approximately 35–40°C, while the temperature in the rectum was within the physiological range during AMF irradiation (35–37°C).

Western Blotting

Transplanted prostate tumor tissue, which was partially resected from the tumor and frozen at sacrifice, was homogenized in RIPA buffer (150 mM NaCl, 50 mM Tris–HCl [pH 8.0], 1% NP-40, 0.5% sodium deoxycholate, 0.1% SDS, 1 mM phenylmethylsulfonyl fluoride, 1 mM sodium orthovanadate, and protease inhibitor cocktail [Complete; Roche, France]). Twenty-microgram aliquots of protein were resolved by SDS–PAGE, and separated proteins were transferred to nitrocellulose membranes and incubated with heat shock protein 70 (HSP70; Cell Signaling Technology, Danvers, MA), cleaved caspase 3 (Cell Signaling

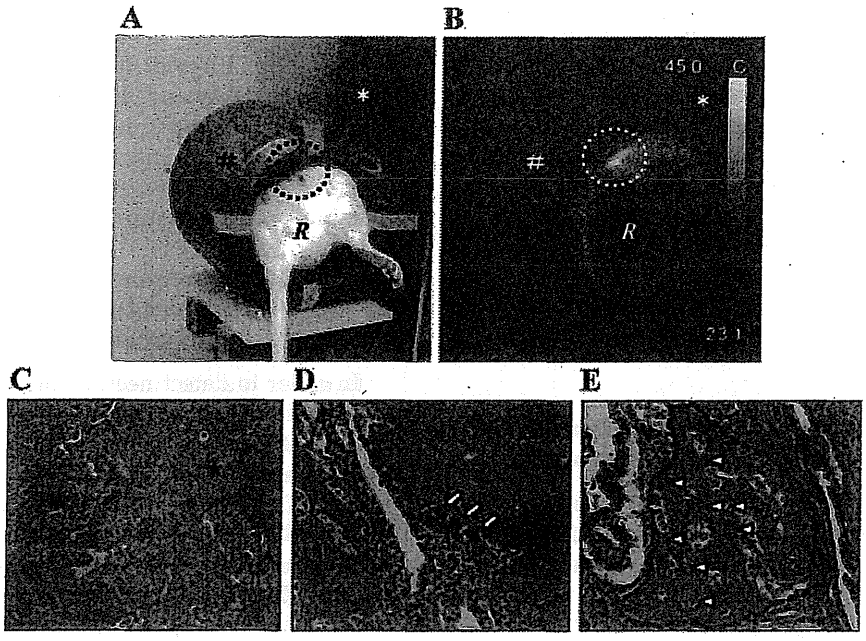

Fig. 1. *Tumor-specific hyperthermia measured by thermography and histopathology in a novel rat model of prostate cancer bone metastasis* (**A**), Alternating magnetic field (AMF) irradiation machine and rat with magnetic cationic liposomes (MCLs) injected into the transplanted tumor. The rat (R) was placed inside the horizontal coil (#) of the AML irradiation machine (*). The area circled with a dotted line indicates the site of the transplanted tumor injected with MCL. **B**: Tumor-specific hyperthermia measured by thermography. The site of MCL injection was at a high temperature (yellow) compared with the temperature of remainder of the rat (orange). **C**: Hematoxylin and eosin (H & E) staining of transplanted prostate cancer. Prostate cancer cells (#) infiltrated the femur (*; magnification, 20×). **D**: Osteoclasts (arrows) are apparent within the growth of prostate cancer cells (#; magnification, 100×). **E**: Osteoblasts (arrowhead) with osteoid (dotted line) are observed with prostate cancer cells (#) (magnification, 100×).

Technology), interleukin-2 (IL-2; Abcam, Cambridge, UK), interferon-gamma (IFN-gamma) (Abcam), or β-actin (AC-74; Sigma–Aldrich, St. Louis, MO) antibodies. Immunoreactions were visualized with the ECL-Plus detection system (GE Healthcare, Piscataway, NJ) after a 1-hr incubation with horseradish peroxidase-labeled anti-mouse secondary antibodies (Cell Signaling Technology).

Immunohistochemical and Histochemical Analysis

Immunohistochemical staining was applied to paraffin-embedded sections (3 μm thick) of transplanted prostate cancer tissues. Sections were incubated for 60 min with antibodies specific to HSP70, proliferating cell nuclear antigen (PCNA; Dako Cytomation Inc., Glostrup, Denmark), CD68 (AbD Serotec, Kidlington, UK), and CD8a (AbD Serotec). Staining was achieved using two-step EnVision + System-HRP methodology, according to the manufacturer's instructions (Dako Cytomation Inc.). The sections were lightly counterstained with hematoxylin to facilitate orientation. Immunostained slides were evaluated by light microscopy, and the proportion of positively stained cells (positivity) was quantified as positive cancer, normal cell nuclei or membrane/total cancer, and normal cell nuclei or membrane. Berlin blue staining was performed to stain MCL particles.

Statistical Analysis

The significance of the data was determined by Student's *t*-test (two-tailed) using SPSS software (SPSS, Chicago, IL). In vivo analysis was performed using the Mann–Whitney *U*-test of significance. $P < 0.05$ was deemed significant.

RESULTS

Establishment of an Animal Model of Bone Metastatic Prostate Cancer

To assess the anti-cancer effects of repeated thermotherapy in the bone microenvironment, we established a novel rat model that mimics human prostate cancer bone metastasis by transplanting prostate cancer cells into the femur. In the bone

microenvironment of this model, bone destruction (Fig. 1C), as well as osteoclast (Fig. 1D) and osteoblast (Fig. 1E) induction, were observed. The rats showed almost no side effects in response to repeated MCL thermotherapy, such as debilitation or weight loss. While the average body weight of rats in the DTX and MCL + DTX groups was significantly decreased compared with the body weights of rats from the control group from day 7 to day 10, no significant differences in weight were observed among the groups by the end of the experimental period.

MCL Thermotherapy Suppressed Prostate Cancer Growth in the Bone Microenvironment

Tumor volume in the MCL + DTX group was significantly suppressed compared to that in the control and DTX groups (Fig. 2A). Tumor volumes from day 0 to day 11 after therapy showed almost no change in any of the groups. To assess cell proliferation, PCNA immunostaining was performed on specimens of transplanted tumor from each group. Although many cancer cells were positively stained in the control group, only a few cancer cells were positively stained in the MCL and MCL + DTX groups (Fig. 2B), and the percentage of PCNA positively stained cancer cells in these groups was significantly lower than that in the control and DTX groups (Fig. 2C). The percentage of PCNA positively stained cancer cells in the DTX group was almost the same as that in the control group (Fig. 2C).

MCL Thermotherapy Induced Prostate Cancer Necrosis and Apoptosis in the Bone Microenvironment

In order to detect necrotic areas in the tumors, we evaluated tumor necrosis by light microscopy and quantified it using an image analyzer. Necrotic areas were observed in prostate cancer tissue in all groups (Fig. 3A). The necrotic areas in the MCL and MCL + DTX groups extended markedly beyond the MCL-injected area indicated by Berlin blue-positive particles (Fig. 3A). When the necrotic areas were measured quantitatively using the IPAP image analyzer (Fig. 3A, green), the area that was necrotic in the tumors from the MCL and MCL + DTX groups was significantly greater by percentage than that in the control group (Fig. 3B). The percentage of necrotic

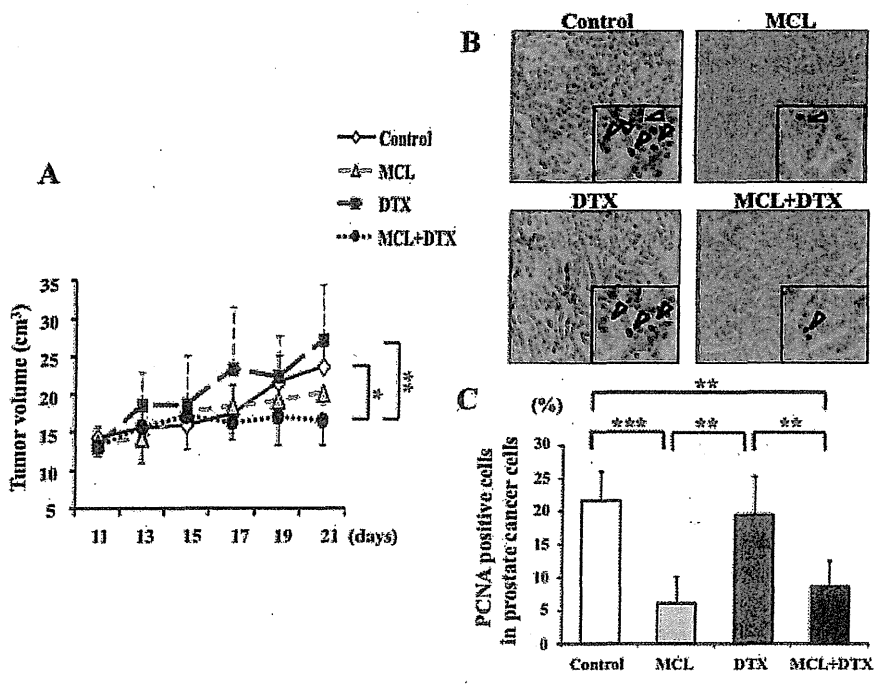

Fig. 2. Tumor growth curve and cell proliferation in a novel rat model of prostate cancer bone metastasis (**A**), sequential changes in transplanted tumor volume (cm^3). Continuous line (◆), dashed spaced line (▲), dashed line (■), and dotted line (●) represent the control group, MCL group, DTX group, and MCL + DTX group, respectively. Values are the mean ± SD ($^*P < 0.05$, $^{**}P < 0.01$). **B**: Immunohistochemistry of PCNA in control, MCL, DTX, and MCL + DTX groups (magnification, 100×; magnification of inclusion photograph, 400×). Positive staining is evident in the nuclei of cancer cells. **C**: PCNA-positive labeling indices. Values are the mean ± SD ($^{**}P < 0.01$, $^{***}P < 0.001$).

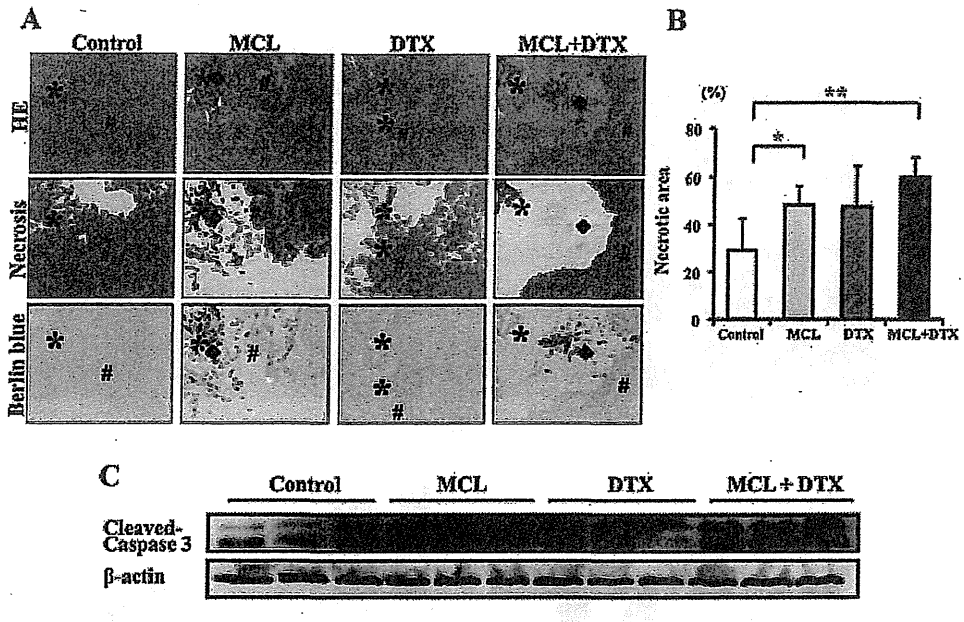

Fig. 3. The evaluation of necrosis and apoptosis in a novel rat model of prostate cancer bone metastasis (**A**), Hematoxylin and eosin (H & E)-stained and Berlin blue-stained tissue sections of transplanted tumors from the control, MCL, DTX, and MCL + DTX groups. Bone (*), MCL (◆), and viable tumor area (#) were noted. Necrotic area was measured with an image analyzer, IPAP (green). In Berlin blue-stained sections, black particles represent MCL particles. (magnification, 20×). **B:** Percentage of necrotic area in the transplanted tumor. Values are the mean ± SD ($^{*}P < 0.05$, $^{**}P < 0.01$). **C:** Cleaved caspase 3 protein expression in transplanted tumors from the control, MCL, DTX, and MCL + DTX groups, as visualized by Western blotting.

area in tumors from the DTX group was also greater than that in the control group, although this difference was not significant (Fig. 3B).

To assess the apoptotic status of the tumor, we evaluated cleaved caspase 3 protein expression in tumors from all four groups. Cleaved caspase 3 expression was observed in the MCL, DTX, and MCL + DTX groups (Fig. 3C), demonstrating that MCL thermotherapy induced necrosis and apoptosis concurrently in the tumors.

MCL Thermotherapy Suppressed Bone Destruction and Osteoclast Induction

Bone destruction is a serious impediment to maintaining the quality of life of patients with bone-metastasized prostate cancer. We examined the effects of MCL and DTX treatment on bone destruction and osteoclast induction in prostate cancer in the bone microenvironment by performing CT and CD68 immunostaining. On CT images, bone destruction was clearly observed in the control group, with less destruction observed in the MCL and MCL + DTX groups (Fig. 4A). Statistically, the remaining bone volume in all treatment groups was greater than that in the control group (Fig. 4B). CD68-positively stained multinuclear cells were also frequently observed in the control and DTX groups, but were scattered in the MCL and MCL + DTX groups (Fig. 4C). When the number of CD68-positive multinuclear cells was determined, tumors from the MCL and MCL + DTX groups were found to have significantly fewer cells than the control and DTX groups (Fig. 4D).

MCL Thermotherapy Induced CD8-Positive Cells, As Well As IL-2, IFN-Gamma, and HSP70 Expression

Previous results have shown that thermotherapy induces tumor immunity. We assessed the induction of tumor immunity in prostate cancer in the bone microenvironment by immunostaining for CD8, which is a marker of cytotoxic T lymphocytes (CTL), the main constituents of tumor immunity. CD8-positive lymphocytes were easily observed in the MCL and MCL + DTX groups compared with the control and DTX groups (Fig. 5A). Statistically, the numbers of CD8-positive lymphocytes in the tumors from the MCL and MCL + DTX groups were significantly increased compared to those in the control and DTX groups (Fig. 5B).

IL-2 and IFN-gamma are known to be cytokines associated with CD8-positive T lymphocytes. We therefore investigated IL-2 and IFN-gamma expression in the tumors by Western blot analysis, and found that

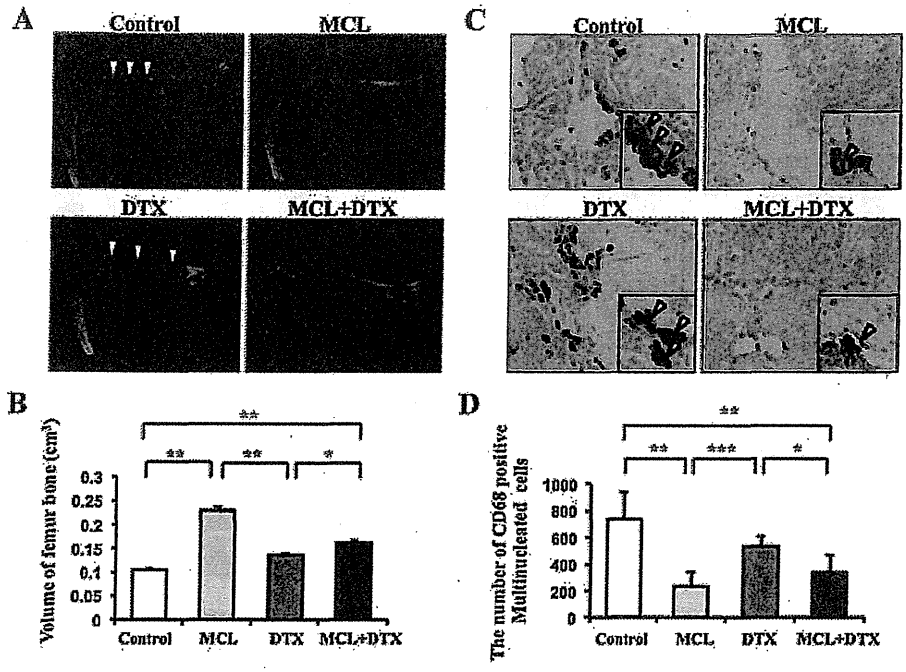

Fig. 4. The evaluation of bone destruction and osteoclast induction in a novel rat model of prostate cancer bone metastasis (**A**), computerized tomography (CT) of rat femur bone with transplanted prostate tumor. The arrowhead indicates destructed femur bone. **B**: Remaining bone volume calculated by CT. Values are the mean ± SD ($^{*}P < 0.05$, $^{**}P < 0.01$). **C**: Immunohistochemistry of CD68 in control, MCL, DTX, and MCL + DTX groups (magnification, 100×; magnification of inclusion photograph, 400×). Positive staining is evident in the cytoplasm and membrane of multinucleated cells. **D**: Number of CD68-positive multinucleated cells of rat femur with transplanted prostate tumor. Values are the mean ± SD ($^{*}P < 0.05$, $^{**}P < 0.01$, $^{***}P < 0.001$).

IL-2 and IFN-gamma protein expression was higher in the tumors from the MCL and MCL + DTX groups than in those from the control and DTX groups (Fig. 5C).

HSP70 is known to be induced by temperature elevation, and to enhance anti-tumor CTL. We therefore investigated HSP70 expression in our model. Using fluorescence immunohistochemistry, HSP70-positive cancer cells were clearly observed in the MCL and MCL + DTX groups, but not in the control and DTX groups. This result was confirmed by Western blot analysis, which showed higher HSP70 protein expression in the tumors from the MCL and MCL + DTX groups than in those from the control and DTX groups (Fig. 5D).

DISCUSSION

Understanding cellular and molecular changes in the bone microenvironment is important for developing novel treatments for prostate cancer bone metastasis. In the bone microenvironment, the growth of metastasized prostate cancer cells is promoted by growth factors secreted to induce bone resorption, which is mediated by osteoclasts [9,26]. Thus, blockade of the vicious cycle between tumor cells and osteoclasts is important for the control of prostate cancer bone metastasis. In this study, we used a novel rat model to examine the efficacy of MCL thermotherapy in the treatment of this disease.

Currently used rodent tumor models, including transgenic tumor models and those in which human tumors are grown subcutaneously in severe combined immunodeficiency (SCID) mice, do not sufficiently represent clinical cancer, especially with regard to metastasis and drug sensitivity. For instance, human prostate cancer cells are commonly transplanted into SCID mice in in vivo experiments examining prostate cancer bone metastasis; however, an investigation into tumor immunity by using such animals is impossible because of their compromised immunocompetence. Rather, the surgical orthotropic transplant (SOI) technique is important in order to obtain clinically accurate models [27,28]. Moreover, a fluorescent SOI model of spontaneous bone metastatic human prostate cancer has previously been reported [29–31]. We therefore employed a novel rat model in this study that maintains normal immunity and allows the evaluation of detailed tumor immunity in vivo, thereby providing an advantage for in vivo investigations. Using this model, we herein demonstrated that

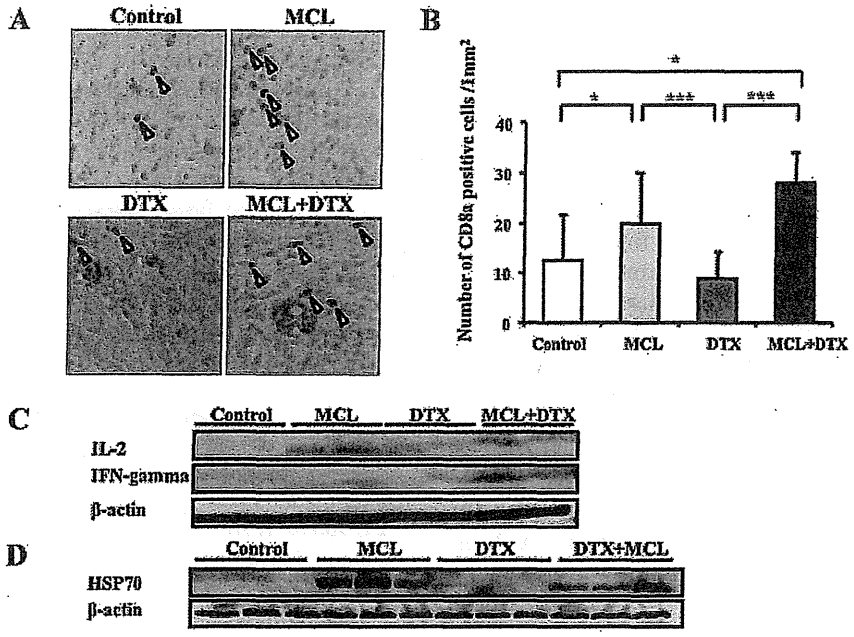

Fig. 5. The evaluation of tumor immunity by the presence of CD8-positive cells and IL-2, IFN-gamma, and HSP70 expression in a novel rat model of prostate cancer bone metastasis (**A**), CD8 immunohistochemistry of the tumor in control, MCL, DTX, and MCL + DTX groups. *Positive staining is evident in the nuclei of lymphocytes (magnification, 40 ×).* **B**: *Number of CD8a-positive cells in the transplanted tumor.* Values are the mean ± SD ($^{*}P < 0.05$, $^{***}P < 0.001$). **C**: Western blot analysis of IL-2 and IFN-gamma expression in transplanted tumors from the control, MCL, DTX, and MCL + DTX groups. **D**: Western blot analysis of HSP70 expression in transplanted tumors from the control, MCL, DTX, and MCL + DTX groups.

MCL thermotherapy in this rat model of prostate cancer bone metastasis induced tumor necrosis and apoptosis, suppressed bone destruction and osteoclast induction, and enhanced tumor immunity against prostate cancer in the bone microenvironment. Moreover, we demonstrated that therapy with MCL in conjunction with DTX significantly inhibited tumor growth. Indeed, when cancer cell death was examined, the area of tumor necrosis was found to be significantly greater in both the MCL and MCL + DTX groups than in the control group. Moreover, the induction of apoptosis was observed in tumors from the MCL, DTX, and MCL + DTX groups. These results demonstrate that combination therapy using MCL thermotherapy and DTX can powerfully induce prostate cancer cell death through the activation of different mechanisms.

Thermotherapy has been demonstrated to induce tumor immunity [32], including in a study that found that tumor immunity is induced by MCL thermotherapy in rat glioma [33]. It has been reported that increased HSP70 expression plays a role in the induction of CTL-mediated tumor immunity [34]. In detail, the uptake of HSP70-binding tumor peptide by MHC class I molecules on tumor cells induces the activation tumor-specific CD8-positive T lymphocytes, which are the major immune cells involved in tumor immunity [35,36]. Moreover, after cell death, HSP70-binding tumor peptide is released and engulfed by antigen-presenting cells such as macrophages, which is thought to further induce CD4-positive T lymphocytes. Although HSP70 is believed to be an exacerbation factor under hyperthermia that protects against apoptosis [37–39], and several previous reports have demonstrated that HSP expression induces heat tolerance in cells and adversely affects thermotherapy [40], MCL thermotherapy did not inhibit apoptosis resulting from DTX treatment in this study (Fig. 3C). This suggests that the induction of apoptosis by DTX might be maintained in combination therapy including both MCL and DTX. In addition to the increased number of CD8-positive cells and increased HSP70 protein expression observed in this study, we showed an increase in the expression of IL-2 and IFN-gamma, which are known to induce CD8-positive T lymphocytes. Therefore, we suggest that MCL thermotherapy induces tumor immunity through the up-regulation of HSP70, IL-2, and IFN-gamma, and the subsequent induction of CD8-positive T lymphocytes.

Although the anticancer drug DTX has been proven effective against castration-resistant prostate cancer, DTX induces weight loss as a side effect of

repeated treatment, thereby limiting the dose and treatment times of DTX-based therapy. In this study, DTX (10 mg/kg) was injected into rats via the tail vein [41], which is an amount the equivalent of five times greater than what is administered to humans. This led to 20% weight loss after 1 week, which required the discontinuation of the second administration of DTX. With regard to the findings from the DTX group in this study, the data from the tumor volume curves are controversial because the tumor volume in the DTX group was almost the same as in the control group (Fig. 2A). This was despite the results of our Western blot analysis for caspase 3 (Fig. 3C), which revealed that DTX was actually effective in inducing apoptosis in the tumor. Moreover, the tumor necrotic area in the DTX group tended to increase compared with that in the control group (Fig. 3B). Thus, although significant reduction of tumor volume was not observed, we consider that the administration of DTX was actually effective for inducing tumor necrosis and apoptosis.

Unlike DTX treatment, MCL thermotherapy heats tumor tissue without damaging neighboring normal tissues, and can therefore be performed safely and repeatedly. However, MCL thermotherapy has several problems that must be resolved before its application in the clinical setting, such as the development of AMF irradiation equipment appropriate for the human body, and an investigation into the safe use of MCLs. The injection of MCLs into tumor tissue becomes easier with the aid of three-dimensional CT or transrectal supersonic wave technology; however, for patients whose overall status is worsening, such as in cases of castration-resistant prostate cancer, administration by intravenous injection would be preferable. Unfortunately, owing to the large size of available MCLs (120–150 nm), intravenous injection is currently impossible. We are therefore attempting to minimize the size of MCLs. Finally, the development of a system capable of effectively guiding MCLs to the tumor region is necessary, and the effects of MCL thermotherapy must be examined using the spontaneous SOI model of metastasis that allows visualization of fluorescent protein prior to clinical application. If these problems can be resolved in the near future, the clinical application of MCL thermotherapy will be possible.

CONCLUSIONS

In summary, MCL thermotherapy heats only tumor tissue injected with MCLs, and is capable of inducing both necrotic and apoptotic cancer cell death, as well as tumor immunity, and suppressing bone destruction. In this study, the MCL thermotherapy group showed inhibition of bone destruction due to osteoclast induction compared with the control and DTX groups. Moreover, MCL thermotherapy inhibited cancer cell proliferation compared with that observed in the control and DTX groups, demonstrating that MCL thermotherapy can treat tumor cells and osteoclasts at the same time, as well as inhibit the vicious cycle of bone metastases. Finally, we showed that the combination of MCL thermotherapy and DTX treatment is much more effective than DTX monotherapy, suggesting that MCL thermotherapy should be adopted as a novel treatment for patients with bone metastatic prostate cancer in the future.

ACKNOWLEDGMENTS

This study was supported by a grant-in-Aid for Scientific Research (C) No. 21592055 and No. 21790390 from the Ministry of Education, Culture, Sports, Science and Technology of Japan, a grant-in-aid for Research at Nagoya City University, a grant-in-aid from Ichihara International Scholarship Foundation, and a grant-in-aid from Aichi Cancer Research Foundation. We thank Noritaka Yoshikawa (Olympus Medical Science Sale Co., Ltd.) who provided CT for animal experiments of bone evaluation and thermography for temperature evaluations. We also thank Koji Kato, Engineer (Department of Experimental Pathology, Nagoya City University Graduate School of Medical Sciences) and Ayano Yoshida (College of Bioscience and Biotechnology, Chubu University) for technical assistance.

REFERENCES

1. Bubendorf L, Schopfer A, Wagner U, Sauter G, Moch H, Willi N, Gasser TC, Mihatsch MJ. Metastatic patterns of prostate cancer: An autopsy study of 1,589 patients. Hum Pathol 2000; 31:578–583.
2. Mehra R, Kumar-Sinha C, Shankar S, Lonigro RJ, Jing X, Philips NE, Siddiqui J, Han B, Cao X, Smith DC, Shah RB, Chinnaiyan AM, Pienta KJ. Characterization of bone metastases from rapid autopsies of prostate cancer patients. Clin Cancer Res 2011;17:3924–3932.
3. Saad F, Clarke N, Colombel M. Natural history and treatment of bone complications in prostate cancer. Eur Urol 2006;49: 429–440.
4. Jemal A, Siegel R, Xu J, Ward E. Cancer statistics, 2010. CA Cancer J Clin 2010;60:277–300.
5. Kingsley LA, Fournier PG, Chirgwin JM, Guise TA. Molecular biology of bone metastasis. Mol Cancer Ther 2007;6:2609–2617.
6. Kozlow W, Guise TA. Breast cancer metastasis to bone: Mechanisms of osteolysis and implications for therapy. J Mammary Gland Biol Neoplasia 2005;10:169–180.
7. Yoneda T, Hiraga T. Crosstalk between cancer cells and bone microenvironment in bone metastasis. Biochem Biophys Res Commun 2005;328:679–687.
8. Finkelman RD, Mohan S, Jennings JC, Taylor AK, Jepsen S, Baylink DJ. Quantitation of growth factors IGF-I, SGF/IGF-II,

and TGF-beta in human dentin. J Bone Miner Res 1990;5: 717–723.

9. Sato S, Futakuchi M, Ogawa K, Asamoto M, Nakao K, Asai K, Shirai T. Transforming growth factor beta derived from bone matrix promotes cell proliferation of prostate cancer and osteoclast activation-associated osteolysis in the bone microenvironment. Cancer Sci 2008;99:316–323.
10. Solheim E. Growth factors in bone. Int Orthop 1998;22:410–416.
11. Berry S, Waldron T, Winquist E, Lukka H. The use of bisphosphonates in men with hormone-refractory prostate cancer: A systematic review of randomized trials. Can J Urol 2006;13:3180–3188.
12. Saad F, McKiernan J, Eastham J. Rationale for zoledronic acid therapy in men with hormone-sensitive prostate cancer with or without bone metastasis. Urol Oncol 2006;24:4–12.
13. Fizazi K, Carducci M, Smith M, Damiao R, Brown J, Karsh L, Milecki P, Shore N, Rader M, Wang H, Jiang Q, Tadros S, Dansey R, Goessl C. Denosumab versus zoledronic acid for treatment of bone metastases in men with castration-resistant prostate cancer: A randomised, double-blind study. Lancet 2011;377:813–822.
14. Kusaka M, Takegami K, Sudo A, Yamazaki T, Kawamura J, Uchida A. Effect of hyperthermia by magnetite cement on tumor-induced bone destruction. J Orthop Sci 2002;7:354–357.
15. Abe M, Hiraoka M, Takahashi M, Egawa S, Matsuda C, Onoyama Y, Morita K, Kakehi M, Sugahara T. Multi-institutional studies on hyperthermia using an 8-MHz radiofrequency capacitive heating device (Thermotron RF-8) in combination with radiation for cancer therapy. Cancer 1986; 58:1589–1595.
16. Kawai N, Futakuchi M, Yoshida T, Ito A, Sato S, Naiki T, Honda H, Shirai T, Kohri K. Effect of heat therapy using magnetic nanoparticles conjugated with cationic liposomes on prostate tumor in bone. Prostate 2008;68:784–792.
17. Kawai N, Ito A, Nakahara Y, Futakuchi M, Shirai T, Honda H, Kobayashi T, Kohri K. Anticancer effect of hyperthermia on prostate cancer mediated by magnetite cationic liposomes and immune-response induction in transplanted syngeneic rats. Prostate 2005;64:373–381.
18. Kawai N, Ito A, Nakahara Y, Honda H, Kobayashi T, Futakuchi M, Shirai T, Tozawa K, Kohri K. Complete regression of experimental prostate cancer in nude mice by repeated hyperthermia using magnetite cationic liposomes and a newly developed solenoid containing a ferrite core. Prostate 2006;66:718–727.
19. Yanase M, Shinkai M, Honda H, Wakabayashi T, Yoshida J, Kobayashi T. Intracellular hyperthermia for cancer using magnetite cationic liposomes: An in vivo study. Jpn J Cancer Res 1998;89:463–469.
20. Shirai T, Tamano S, Kato T, Iwasaki S, Takahashi S, Ito N. Induction of invasive carcinomas in the accessory sex organs other than the ventral prostate of rats given 3,2'-dimethyl-4-aminobiphenyl and testosterone propionate. Cancer Res 1991; 51:1264–1269.
21. Sato S, Takahashi S, Asamoto M, Naiki T, Naiki-Ito A, Asai K, Shirai T. Tranilast suppresses prostate cancer growth and osteoclast differentiation in vivo and in vitro. Prostate 2010;70:229–238.
22. Owen CS, Sykes NL. Magnetic labeling and cell sorting. J Immunol Methods 1984;73:41–48.
23. Shinkai M, Yanase M, Honda H, Wakabayashi T, Yoshida J, Kobayashi T. Intracellular hyperthermia for cancer using magnetite cationic liposomes: In vitro study. Jpn J Cancer Res 1996;87:1179–1183.
24. Sorensen AG, Patel S, Harmath C, Bridges S, Synnott J, Sievers A, Yoon YH, Lee EJ, Yang MC, Lewis RF, Harris GJ, Lev M, Schaefer PW, Buchbinder BR, Barest G, Yamada K, Ponzo J, Kwon HY, Gemmete J, Farkas J, Tievsky AL, Ziegler RB, Salhus MR, Weisskoff R. Comparison of diameter and perimeter methods for tumor volume calculation. J Clin Oncol 2001;19:551–557.
25. Jensen MM, Jorgensen JT, Binderup T, Kjaer A. Tumor volume in subcutaneous mouse xenografts measured by microCT is more accurate and reproducible than determined by 18F-FDG-microPET or external caliper. BMC Med Imaging 2008;8:16.
26. Mundy GR. Metastasis to bone: Causes, consequences and therapeutic opportunities. Nat Rev Cancer 2002;2:584–593.
27. Fu X, Herrea H, Hoffman RM. Orthotopic growth and metastasis of human prostate carcinoma in nude mice after transplantation of histologically intact tissue. Int J Cancer 1992;52:987–990.
28. Hoffman RM. Orthotopic metastatic mouse models for anticancer drug discovery and evaluation: A bridge to the clinic. Invest New Drugs 1999;17:343–359.
29. Yang M, Jiang P, Yamamoto N, Li L, Geller J, Moossa AR, Hoffman RM. Real-time whole-body imaging of an orthotopic metastatic prostate cancer model expressing red fluorescent protein. Prostate 2005;62:374–379.
30. Hoffman RM. The multiple uses of fluorescent proteins to visualize cancer in vivo. Nat Rev Cancer 2005;5:796–806.
31. Hoffman RM, Yang M. Whole-body imaging with fluorescent proteins. Nat Protoc 2006;1:1429–1438.
32. Mukhopadhaya A, Mendecki J, Dong X, Liu L, Kalnicki S, Garg M, Alfieri A, Guha C. Localized hyperthermia combined with intratumoral dendritic cells induces systemic antitumor immunity. Cancer Res 2007;67:7798–7806.
33. Ito A, Shinkai M, Honda H, Yoshikawa K, Saga S, Wakabayashi T, Yoshida J, Kobayashi T. Heat shock protein 70 expression induces antitumor immunity during intracellular hyperthermia using magnetite nanoparticles. Cancer Immunol Immunother 2003;52:80–88.
34. Radons J, Multhoff G. Immunostimulatory functions of membrane-bound and exported heat shock protein 70. Exerc Immunol Rev 2005;11:17–33.
35. Udono H, Levey DL, Srivastava PK. Cellular requirements for tumor-specific immunity elicited by heat shock proteins: Tumor rejection antigen gp96 primes CD8+ T cells in vivo. Proc Natl Acad Sci USA 1994;91:3077–3081.
36. Suto R, Srivastava PK. A mechanism for the specific immunogenicity of heat shock protein-chaperoned peptides. Science 1995;269:1585–1588.
37. Subjeck JR, Sciandra JJ, Chao CF, Johnson RJ. Heat shock proteins and biological response to hyperthermia. Br J Cancer Suppl 1982;5:127–131.
38. Subjeck JR, Sciandra JJ, Johnson RJ. Heat shock proteins and thermotolerance; A comparison of induction kinetics. Br J Radiol 1982;55:579–584.
39. Lindquist S. The heat-shock response. Annu Rev Biochem 1986;55:1151–1191.
40. Horowitz M, Robinson SD. Heat shock proteins and the heat shock response during hyperthermia and its modulation by altered physiological conditions. Prog Brain Res 2007;162: 433–446.
41. Wonganan P, Zamboni WC, Strychor S, Dekker JD, Croyle MA. Drug–virus interaction: Effect of administration of recombinant adenoviruses on the pharmacokinetics of docetaxel in a rat model. Cancer Gene Ther 2009;16:405–414.

RESEARCH ARTICLE

Ellagic Acid Inhibits Migration and Invasion by Prostate Cancer Cell Lines

Pornsiri Pitchakarn[1,2], Teera Chewonarin[1,2], Kumiko Ogawa[2,3], Shugo Suzuki[2], Makoto Asamoto[2], Satoru Takahashi[2], Tomoyuki Shirai[2], Pornngarm Limtrakul[1]*

Abstract

Polyphenolic compounds from pomegranate fruit extracts (PFEs) have been reported to possess antiproliferative, pro-apoptotic, anti-inflammatory and anti-invasion effects in prostate and other cancers. However, the mechanisms responsible for the inhibition of cancer invasion remain to be clarified. In the present study, we investigated anti-invasive effects of ellagic acid (EA) in androgen-independent human (PC-3) and rat (PLS10) prostate cancer cell lines *in vitro*. The results indicated that non-toxic concentrations of EA significantly inhibited the motility and invasion of cells examined in migration and invasion assays. The EA treatment slightly decreased secretion of matrix metalloproteinase (MMP)-2 but not MMP-9 from both cell lines. We further found that EA significantly reduced proteolytic activity of collagenase/gelatinase secreted from the PLS-10 cell line. Collagenase IV activity was also concentration-dependently inhibited by EA. These results demonstrated that EA has an ability to inhibit invasive potential of prostate cancer cells through action on protease activity.

Key words: Ellagic acid - cancer - invasion - migration - metastasis

Asian Pacific J Cancer Prev, **14** (5), 2859-2863

Introduction

Prostate cancer is the most common male malignant tumor in the Western countries (Gronberg, 2003). The 5-year survival rate for the localized disease is close to 90% to 100%, while just approximately 32% for the metastatic prostate cancer (Jemal et al., 2008). The major cause of deaths is due to the complications resulting from cancer metastases to distant organs in the body, and treatment of such metastatic disease is one of the major therapeutic challenges. Prostate cancer growth is initially androgen-dependent, medical or surgical castration has been the standard treatment for metastatic prostate cancer. However, the effect of hormonal therapy is temporary, and most tumors become androgen refractory, which obstacle in the treatment of metastatic prostate cancer.

Cancer metastasis is an important aspect necessary for tumor development, proceeds through a multi-step process, including cellular adhesion and invasion through the basement membrane. The ability of infiltration allows malignant cells to invade other organs through the blood stream or lymph vessels (Fidler and Kripke, 1977; Nagase and Woessner, 1999). Therefore, the prevention of tumor metastasis is one of the goals for cancer patients, and cytotoxic agents have been applied in tumor metastasis therapies. However, such therapy has many serious side effects that could diminish the quality of life in cancer patients (Braun-Falco et al., 2006). Recently, many efforts have been made to reduce the spread of malignant tumors; focused on cell invasion using substances in dietary and medicinal plants, because non- or low-cytotoxic agents are required for tumor metastasis therapy (Yodkeeree et al., 2008; Lin et al., 2009; Pitchakarn et al., 2010).

Ellagic acid (EA) is a polyphenolic compound and present in fruits and berries such as pomegranates, strawberries, raspberries and blackberries. It has anticarcinogenic, antioxidant and antifibrosis properties (Mukhtar et al., 1988; Thresiamma and Kuttan, 1996; Stoner and Gupta, 2001; Han et al., 2006). The anti-carcinogenic effect of EA was shown in several cancer types including esophageal, colon, skin, breast and prostate cancers (Stoner and Gupta, 2001; Larrosa et al., 2006; Bell and Hawthorne, 2008; Strati et al., 2009).

*[1]Department of Biochemistry, Faculty of Medicine, Chiang Mai University, Chiang Mai, Thailand, [2]Department of Experimental Pathology and Tumor Biology, Nagoya City University, Graduate School of Medical Sciences, Nagoya, [3]Division of Pathology, National Institute of Health Sciences, Tokyo, Japan *For correspondence: plimtrak@med.cmu.ac.th*

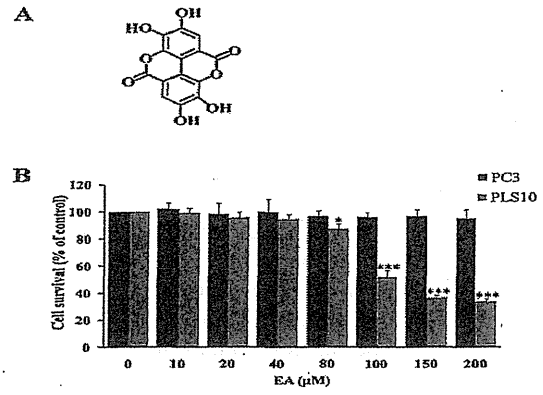

Figure 1. The Cell Growth Effect of EA on PC3 and PLS10. A) The structure of EA. B) The cells were incubated with various concentration of EA for 48 h and then the cell growth was assessed by WST-1 assay. The results are expressed as a percentage of the untreated cell (0 μM). *, ***significantly different from 0 μM at $p<0.05$ and 0.001, respectively

It was found that EA could be detected in plasma and accumulated in the intestine and prostate (Larrosa, Tomas-Barberan and Espin, 2006; Seeram et al., 2006; 2007). The amount of information available on the properties and roles of pomegranate extracts including EA is very limited, their potential as chemopreventive and chemotherapeutic agents of cancers needs to be achieved. The present study, we investigated the effect of EA on the invasion of androgen-independent human (PC3) and rat (PLS10) prostate cancer cell lines.

Materials and Methods

Chemicals and cell culture

Ellagic acid, which structure is presented in Fig. 1A, was purchased from Fluka Co.Ltd., Germany. Androgen-independent prostate cancer cell lines, PC-3 (human) which purchased from The American Type Culture Collection (ATCC, Manassas, VA, USA) and PLS10 (rat) that has been established from 3,2'–dimethyl-4-aminobiphenyl plus testosterone-induced carcinomas in the dorsolateral prostate of male F344 rats (Nakanishi, 1996), were used in this study. The cells were cultured in Roswell Park Memorial Institute-1640 Medium (RPMI 1640, Gibco, Carlsbad, CA, USA) plus 10% fetal bovine serum (FBS, Life Technologies Japan Ltd., Japan), 50 U/ml penicillin and 50 μg/ml streptomycin, maintained in a humidified incubator with an atmosphere comprising 95% air and 5% CO_2 at 37°C. When the cells reach 70-80% confluence, they were harvested and plated either for subsequent passages or for treatments.

Cytotoxicity and growth inhibition assay

The cells were plated at 2.5×10^3 cells per well in 96-well plates. After 24 h, various concentrations of EA were added into the wells. The cells were incubated for 48 h at 37°C, then cell growth were assessed by soluble formazan formation, WST-1 colorimetric assay (Roche, Mannheim Germany) (Hamasaki et al., 1996). In each experiment, determinations were carried out in triplicate.

Invasion and migration assay

The cells were seeded on BD BiocoatTM MatrigelTM invasion or migration (BD Falcon insert) chambers (BD Biosciences, Qume Drive San Jose, California USA), with or without EA at indicated concentrations (25 and 50 μM), and incubated at 37°C. For PC3 cells, cells were incubated for 24h, and 10 μg/ml of fibronectin was used as a chemoattractant. For PLS10 cells, cells were incubated for 48h, and 5% fetal bovine serum was used as a chemoattractant. For migration assay, the cells were treated with EA at the concentration of 0, 25 and 50 μM, and incubated for 24 h. Ten μg/ml of fibronectin or 5% fetal bovine serum were used as a chemoattractants for PC3 or PLS10 cells, respectively. The invading or migrating cells were fixed with 100% ethanol for 5 minutes, then stained with 0.5% crystal violet in 20% methanol for 30 minutes and determined areas by ImageJ 1.410 (National Institute of Mental Health, Bethesda Maryland, USA).

Gelatin zymography

The cells were maintained in serum free RPMI 1640 for 24 h then treated with various concentrations of EA. MMP-2 and MMP-9 secretions from PC3 and PLS10 in the conditioned medium were detected by gelatin zymography as previously described (Fernandez-Patron et al., 1999). The samples were subjected to sodium dodecyl sulfate polyacrylamide gel electrophoresis (SDS-PAGE) using a 10% acrylamide gel containing 0.1 mg/ml of gelatin (Bio-Rad Laboratories, Hercules, California USA) under non-reducing condition. After electrophoresis, SDS in the gel was washed twice with 2.5% Triton-X 100 then incubated at 37°C in the incubating buffer (50 mmol/L Tris-HCl, 200 mmol/L NaCl, and 10 mmol/L $CaCl_2$, pH 7.4) for 24 h. After incubation, the gel was stained with 0.1% Coomassie brilliant blue R250 (Bio-Rad Laboratories) in 50% methanol/10% acetic acid, and destained with 10% acetic acid/50% methanol. The bands of gelatinolytic activity were analyzed using ImageJ 1.410.

Measurement of purified collagenase IV and collagenase/gelatinase secreted from PLS10 activities

An EnzChek Gelatinase/Collagenase Assay Kit (Life Technologies Japan Ltd., Tokyo, Japan.) was used for measuring gelatinase/collagenase activity. PLS10 at 106 cells were cultured in FBS-free DMEM for 24 hours, and then the culture supernatant was collected. The substrate, DQTM fluorescein-conjugate gelatin, was incubated with culture medium of PLS10 or collagenase type IV from Clostridium histolyticum with EA (0, 25, 50 and 100 μg/ml) for 1.5 h and fluorescence signal representing proteolytic activity was measured using a fluorescence microplate reader (480/530 nm).

Statistical analysis

All experiments were done at least in triplicate to see the reproducible. All data presented mean±S.D. Statistical comparisons were performed with one-way ANOVA followed by the Dunnett's test. Statistical significance was concluded with $p<0.05$.

Results

Effect of EA on the cell growth of PC3 and PLS10 cells

WST-1 assay showed that EA treatment caused the reduction of cell growth of PLS10 with inhibitory concentration (IC) 50 about 100 μM while the treatment of EA up to 200 μM did not affect the cell growth of PC3 (Figure 1B). The range of non-toxic concentration was applied in all subsequent experiments.

EA inhibited the invasion and migration of the prostate cancer cells

The invading cells in chambers were presented in Figure 2A which indicates that EA treatment inhibited the invasion of PC3 and PLS10 cells. The inhibition rate in PC3 was approximately 57% and 78%, and in PLS10 by up to 39% and 52%, with 25 and 50 μM of EA treatment, respectively (Figure 2B). Besides, the same concentration of EA also dramatically reduced the motility of the cancer cells. The inhibition rate in PC3 was about 41% and 77%, and in PLS10 by up to 13% and 67%, with 25 and 50 μM of EA, respectively (Figure 3A and 3B).

EA did not affect the secretion of MMP-2, MMP-9 from PC3 and PLS10 cells

Zymography showed that the secretion of MMP-9 from both PC3 and PLS10 cells were not reduced by EA treatment. Meanwhile, MMP-2 (active-form) secretion from the cells was slightly reduced with 50 μM of EA treatment (Figure 4A and 4B). Collectively, these results indicated that EA did not inhibit the cancer cells invasion through the regulation of MMP-2 and MMP-9 secretion.

Effect of EA on the activity of collagenase/gellatinase

Several MMPs exhibit the activity of collagenase and/or gellatinase, the changing activity of collagenase/gellatinase in culture supernatant of PLS10 treated with EA were measured. Comparing to non-treated cells, the activity of collagenase/gellatinase was significantly decreased 24%, 36% and 49% in the culture supernatant of PLS10 treated with EA 25, 50 and 100 μM, respectively (Figure 5A). Moreover, the proteolytic activity of purified collagenase type IV was significantly

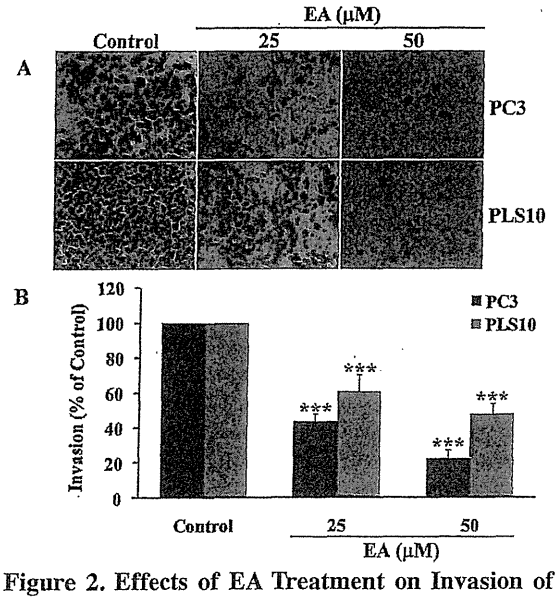

Figure 2. Effects of EA Treatment on Invasion of Prostate Cancer Cell Lines. The cells were photographed under phase-contrast microscopy (A) and quantified (B). The results are expressed as a percentage of the control (0 μM). ***significantly different from the control at $p<0.001$

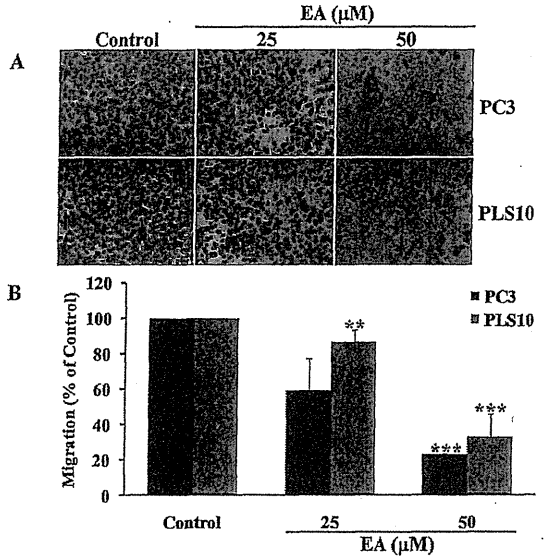

Figure 3. Effects of EA Treatment on Migration of Prostate Cancer Cell Lines. The cells were photographed under phase-contrast microscopy (A) and quantified (B). The results are expressed as a percentage of the control (0 μM). **, ***significantly different from the control at $p<0.01$ and 0.001, respectively

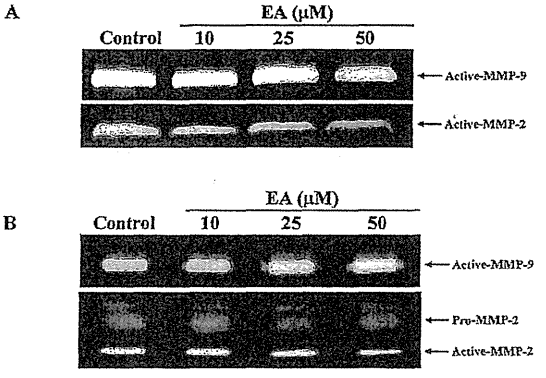

Figure 4. Effects of EA on Secretion of MMP-2 and MMP-9 from PC3 and PLS10 Cells. Secretion of MMP-2 (progenitor and active forms) and MMP-9 in the medium of PC3 (A) and PLS10 cells (B) is shown

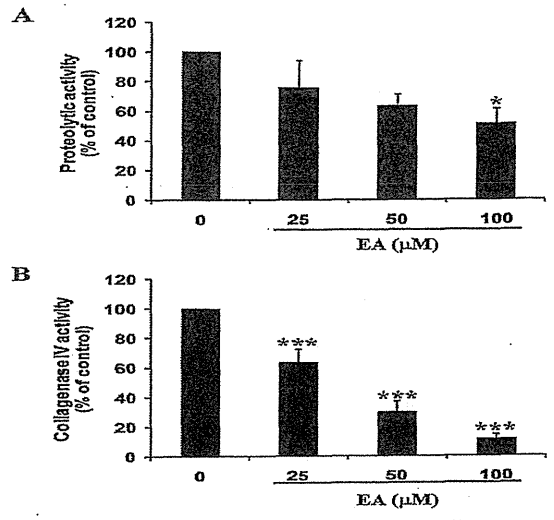

Figure 5. Effects of EA on Activity of Collagenase/ Gelatinase Secreted from PLS10 cells (A) and Purified Collagenase Type IV from *Clostridium histolyticum* (B). The results are expressed as a percentage of the control (0 μM). *, ***significantly different from 0 μM at $p<0.05$ and 0.001, respectively

inhibited by up to 32%, 68% and 87% with 25, 50 and 100 μM of EA, respectively (Figure 5B).

Discussion

EA has been shown to have a biological effect on prostate cancer cells both *in vitro* and *in vivo*. It has been shown to initiate cell cycle arrest, apoptosis and anti-tumorigenic activity in animal models (Castonguay, 1997; Longtin, 2003; Seeram et al., 2005; Bell and Hawthorne, 2008). It can also induce cell-cycle arrest and apoptosis in other cancer types, such as human cervical, bladder and leukemia cells maintained in culture (Narayanan et al., 1999; Li et al., 2005; Khanduja et al., 2006).

The important aspect of high incidence of morbidity and mortality in prostate cancer is tumor invasiveness and metastasis. Metastasis is a complex cascade, accompanied by various physiological alterations involved in extracellular matrix (ECM) degradation, which allows cancer cells to invade blood or lymphatic system spreading to another tissue or organ. Recently, it has been reported that EA inhibited the invasion of human androgen-independent prostate cancer, PC3 cells, *in vitro* (Lansky et al., 2005), however, the mechanism which related to the inhibition remains unclear. The present study, treatment with non-toxic concentration of EA on androgen-independent prostate cancer, PC3 and PLS10 cells markedly reduced the motility and the invasion of the cells. Previous study reported that cells-ECM interactions are premised to be essential for invasion, migration, and metastasis of tumors (Liotta et al., 1986; Azzam and Thompson, 1992; Gilles et al., 1997; Westermarck and Kahari, 1999). MMPs, play a key role in ECM degradation for tumor growth, angiogenesis and invasion (Westermarck and Kahari, 1999). Among MMPs, MMP-2 and MMP-9 have been reported to be the most important for degradation of type IV collagen, a major component of basement membrane (Stetler-Stevenson, 1990; Giancotti and Ruoslahti, 1999; Zeng et al., 1999) and correlated with an aggressive, invasive or metastatic tumor phenotype (Bianco et al., 1998; Cockett et al., 1998; Papathoma et al., 2001; Wang et al., 2003). Therefore, MMP-2 and MMP-9 are afforded to be therapeutic targets of anticancer drugs. We found that EA treatment did not significantly affect the secretions of MMP-2 and MMP-9 from the cells by gelatin zymography. It revealed that the inhibition of EA on the cells invasion might not via the reduction of MMP-2 and MMP-9 secretions. Therefore, the inhibitory effect of EA on broad collagenase/gelatinase was determined. Interestingly, EA exhibited the inhibitor properties against the collagenase/gelatinase secreted from PLS10 cells and also the purified collagenase type IV.

Several articles revealed that MMPs are secreted by tumor cells themselves or by surrounding stromal cells stimulated by the nearby tumor. Numerous studies have linked altered MMP expression in different human cancers with poor prognosis. MMP-1, -2, -3, -7, -9, -13 and -14 all have elevated expression in primary and/or metastasis tumor, while up-regulation of MMPs lead to enhanced cancer cell invasion. From these results, we can conclude that EA had ability to reduce the invasiveness of prostate cancer cell lines by the modulation of MMP activity. Therefore, EA might be used as an adjuvant therapy for prostate cancer.

Acknowledgement

This work was supported by Faculty of Medicine Research Fund, Chiang Mai University, Chiang Mai, Thailand and the Society for Promotion of Pathology of Nagoya, Japan.

References

Azzam HS, Thompson EW (1992). Collagen-induced activation of the M(r) 72,000 type IV collagenase in normal and malignant human fibroblastoid cells. *Cancer Res*, **52**, 4540-4.

Bell C, Hawthorne S (2008). Ellagic acid, pomegranate and prostate cancer -- a mini review. *J Pharm Pharmacol*, **60**, 139-44.

Bianco FJ Jr, Gervasi DC, Tiguert R, et al (1998). Matrix metalloproteinase-9 expression in bladder washes from bladder cancer patients predicts pathological stage and grade. *Clin Cancer Res*, **4**, 3011-6.

Braun-Falco M, Holtmann C, Lordick F, et al (2006). Follicular drug reaction from cetuximab: a common side effect in the treatment of metastatic colon carcinoma. *Hautarzt*, **57**, 701-4.

Castonguay AGHU, Perchellet EM (1997). Antitumorigenic and antipromoting activities of ellagic acid, ellagitannins and oligometric anthocyanin and procyanidin. *Int J Oncol*, **10**, 367-73.

Cockett MI, Murphy G, Birch ML, et al (1998). Matrix metalloproteinases and metastatic cancer. *Biochem Soc Symp*, **63**, 295-313.

Fernandez-Patron C, Radomski MW, Davidge ST (1999). Vascular matrix metalloproteinase-2 cleaves big endothelin-1 yielding a novel vasoconstrictor. *Circ Res*, **85**, 906-11.

Fidler IJ, Kripke ML (1977). Metastasis results from preexisting variant cells within a malignant tumor. *Science*, **197**, 893-5.

Giancotti FG, Ruoslahti E (1999). Integrin signaling. *Science*, **285**, 1028-32.

Gilles C, Polette M, Seiki M, et al (1997). Implication of collagen type I-induced membrane-type 1-matrix metalloproteinase expression and matrix metalloproteinase-2 activation in the metastatic progression of breast carcinoma. *Lab Invest*, **76**, 651-60.

Gronberg H (2003). Prostate cancer epidemiology. *Lancet*, **361**, 859-64.

Hamasaki K, Kogure K, Ohwada K (1996). A biological method for the quantitative measurement of tetrodotoxin (TTX): tissue culture bioassay in combination with a water-soluble tetrazolium salt. *Toxicon*, **34**, 490-5.

Han DH, Lee MJ, Kim JH (2006). Antioxidant and apoptosis-inducing activities of ellagic acid. *Anticancer Res*, **26**, 3601-6.

Jemal A, Siegel R, Ward E, et al (2008). Cancer statistics, 2008. *CA Cancer J Clin*, **58**, 71-96.

Khanduja KL, Avti PK, Kumar S, et al (2006). Anti-apoptotic activity of caffeic acid, ellagic acid and ferulic acid in normal human peripheral blood mononuclear cells: a Bcl-2 independent mechanism. *Biochim Biophys Acta*, **1760**, 283-9.

Lansky EP, Harrison G, Froom P, et al (2005). Pomegranate (*Punica granatum*) pure chemicals show possible synergistic inhibition of human PC-3 prostate cancer cell invasion across Matrigel. *Invest New Drugs*, **23**, 121-2.

Larrosa M, Tomas-Barberan FA, Espin JC (2006). The dietary hydrolysable tannin punicalagin releases ellagic acid that induces apoptosis in human colon adenocarcinoma Caco-2 cells by using the mitochondrial pathway. *J Nutr Biochem*, **17**, 611-25.

Lin SS, Lai KC, Hsu SC, et al (2009). Curcumin inhibits the migration and invasion of human A549 lung cancer cells through the inhibition of matrix metalloproteinase-2 and -9 and vascular endothelial growth gactor (VEGF). *Cancer Lett*, **285**, 127-33.

Liotta LA, Rao CN, Wewer UM (1986). Biochemical interactions of tumor cells with the basement membrane. *Annu Rev Biochem*, **55**, 1037-57.

Li TM, Chen GW, Su CC, et al (2005). Ellagic acid induced p53/p21 expression, G1 arrest and apoptosis in human bladder cancer T24 cells. *Anticancer Res*, **25**, 971-9.

Longtin R (2003). The pomegranate: nature's power fruit? *J Natl Cancer Inst*, **95**, 346-8.

Mukhtar H, Das M, Khan WA, et al (1988). Exceptional activity of tannic acid among naturally occurring plant phenols in protecting against 7,12-dimethylbenz(a) anthracene-, benzo(a)pyrene-, 3-methylcholanthrene-, and N-methyl-N-nitrosourea-induced skin tumorigenesis in mice. *Cancer Res*, **48**, 2361-5.

Nagase H, Woessner JF, Jr. (1999). Matrix metalloproteinases. *J Biol Chem*, **274**, 21491-4.

Nakanishi HTS, Kato K, Shimizu S, et al (1996). Establishment and characterization of three androgen-independent, metastatic carcinoma cell lines from 3,2'-dimethyl-4-aminobiphenyl-induced prostatic tumors in F344 rats. *Jpn J Cancer Res*, **87**, 1218-26.

Narayanan BA, Geoffroy O, Willingham MC, et al (1999). p53/p21(WAF1/CIP1) expression and its possible role in G1 arrest and apoptosis in ellagic acid treated cancer cells. *Cancer Lett*, **136**, 215-21.

Papathoma AS, Zoumpourlis V, Balmain A, et al (2001). Role of matrix metalloproteinase-9 in progression of mouse skin carcinogenesis. *Mol Carcinog*, **31**, 74-82.

Pitchakarn P, Ogawa K, Suzuki S, et al (2010). Momordica charantia leaf extract suppresses rat prostate cancer progression *in vitro* and *in vivo*. *Cancer Sci*, **101**, 2234-40.

Seeram NP, Adams LS, Henning SM, et al (2005). *In vitro* antiproliferative, apoptotic and antioxidant activities of punicalagin, ellagic acid and a total pomegranate tannin extract are enhanced in combination with other polyphenols as found in pomegranate juice. *J Nutr Biochem*, **16**, 360-7.

Seeram NP, Henning SM, Zhang Y, et al (2006). Pomegranate juice ellagitannin metabolites are present in human plasma and some persist in urine for up to 48 hours. *J Nutr*, **136**, 2481-5.

Seeram NP, Aronson WJ, Zhang Y, et al (2007). Pomegranate ellagitannin-derived metabolites inhibit prostate cancer growth and localize to the mouse prostate gland. *J Agric Food Chem*, **55**, 7732-7.

Stetler-Stevenson WG (1990). Type IV collagenases in tumor invasion and metastasis. *Cancer Metastasis Rev*, **9**, 289-303.

Stoner GD, Gupta A (2001). Etiology and chemoprevention of esophageal squamous cell carcinoma. *Carcinogenesis*, **22**, 1737-46.

Strati A, Papoutsi Z, Lianidou E, et al (2009). Effect of ellagic acid on the expression of human telomerase reverse transcriptase (hTERT) alpha+beta+ transcript in estrogen receptor-positive MCF-7 breast cancer cells. *Clin Biochem*, **42**, 1358-62.

Thresiamma KC, Kuttan R (1996). Inhibition of liver fibrosis by ellagic acid. *Indian J Physiol Pharmacol*, **40**, 363-6.

Wang M, Wang T, Liu S, et al (2003). The expression of matrix metalloproteinase-2 and -9 in human gliomas of different pathological grades. *Brain Tumor Pathol*, **20**, 65-72.

Westermarck J, Kahari VM (1999). Regulation of matrix metalloproteinase expression in tumor invasion. *FASEB J*, **13**, 781-92.

Yodkeeree S, Garbisa S, Limtrakul P (2008). Tetrahydrocurcumin inhibits HT1080 cell migration and invasion via downregulation of MMPs and uPA. *Acta Pharmacol Sin*, **29**, 853-60.

Zeng ZS, Cohen AM, Guillem JG (1999). Loss of basement membrane type IV collagen is associated with increased expression of metalloproteinases 2 and 9 (MMP-2 and MMP-9) during human colorectal tumorigenesis. *Carcinogenesis*, **20**, 749-55.

Experimental and Toxicologic Pathology 65 (2013) 1035–1041

Contents lists available at ScienceDirect

Experimental and Toxicologic Pathology

journal homepage: www.elsevier.de/etp

Apocynin, an NADPH oxidase inhibitor, suppresses progression of prostate cancer via Rac1 dephosphorylation

Shugo Suzuki[a,b,*], Pornsiri Pitchakarn[a,c], Shinya Sato[a], Tomoyuki Shirai[a], Satoru Takahashi[a]

[a] Department of Experimental Pathology and Tumor Biology, Graduate School of Medicine, Nagoya City University, Nagoya, Japan
[b] Pathology Division, Nagoya City East Medical Center, Nagoya, Japan
[c] Department of Biochemistry, Faculty of Medicine, Chiang Mai University, Chiang Mai, Thailand

ARTICLE INFO

Article history:
Received 8 January 2013
Accepted 31 March 2013

Keywords:
NADPH oxidase
Prostate cancer
Apocynin
Cancer progression
Rac1

ABSTRACT

Recently, considerable evidence has been generated that oxidative stress contributes to the etiology and pathogenesis of prostate cancer. The present study focused on the effects of apocynin, an inhibitor of the NADPH oxidase which generates intracellular superoxide, on a rat androgen-independent prostate cancer cell line (PLS10) in vitro and in vivo. Apocynin significantly inhibited cell proliferation of PLS10 cells via G1 arrest of the cell cycle in vitro. Surprisingly, it did not affect reactive oxygen species (ROS) but inhibited phosphorylation of Rac1, one component of the NADPH oxidase complex. A Rac1 inhibitor, NSC23766, also inhibited cell proliferation, and both apocynin and NSC23766 reduced phosphorylation of Rac1 and NF-κB, as well as cyclin D1. Furthermore, in a xenograft model of prostate cancer with PLS10, apocynin suppressed tumor growth and metastasis in a dose dependent manner in vivo, with reduction of cell proliferation and vessel number in the tumors. Expression and secretion of vascular endothelial growth factor (VEGF) were reduced by apocynin treatment in vivo and in vitro, respectively. In conclusion, despite no apparent direct relationship with oxidative stress, apocynin inhibited growth of androgen-independent prostate cancer in vitro and in vivo. Apocynin thus warrants further attention as a potential anti-tumor drug.

1. Introduction

Prostate cancer is the second most frequently diagnosed cancer in males in the world, with especially higher incidences in Oceania, Europe and North America. In Japan, incident and mortality rates of prostate cancer are relatively low but increasing (Jemal et al., 2011; Damber and Aus, 2008). Androgen ablation therapy is a widely used treatment during the initial stage of the disease and may produce an initially favorable outcome, but most patients eventually develop androgen-independent prostate cancers with metastatic foci, which cause patient death. Currently, there is no therapy that is able to cure progressive hormone-refractory metastatic prostate cancer (Damber and Aus, 2008). New therapeutic agents are thus needed urgently.

Reactive oxygen species (ROS) can be important factors for carcinogenesis and tumor progression, not only inducing DNA damage but also producing cellular alterations such as up-regulation of mitogen activated protein kinase (MAPK) and protein kinase C (PKC) (Lee et al., 2006; Wu, 2006). Recently, considerable evidence has been published suggesting oxidative stress contributes to the etiology and pathogenesis of the prostate cancer (Kumar et al., 2008; Khandrika et al., 2009). Therefore, we have focused on inhibition of ROS production as an anti-tumor approach for prostate cancer.

ROS is produced by mitochondria, peroxisomes, cytochrome P-450, and other cellular elements as a by-product, generated by nicotinamide adenine dinucleotide phosphate (NADPH) oxidase, which is also implicated in a variety of signaling events, including cell growth, cell survival and cell death (Bedard and Krause, 2007). NADPH oxidase consists of phox units ($gp91^{phox}$, $p22^{phox}$, $p40^{phox}$, $p47^{phox}$, $p67^{phox}$) and Rac, the small molecular weight G protein (Bedard and Krause, 2007). Apocynin, a methoxy-substituted catechol that inhibits NADPH oxidase by blocking the association of $p47^{phox}$ and $p67^{phox}$ with $gp91^{phox}$ (Stolk et al., 1994), is now used as a standard NOX inhibitor for research purposes (Bedard and Krause, 2007). Additionally, apocynin can be converted by peroxidase-mediated oxidation to a dimer, which has been shown to be more efficient inhibitor than apocynin itself (Stefanska and Pawliczak, 2008). We previously presented evidence that apocynin reduced oxidative stress induced by arsenite treatment of rat urothelium in vivo (Suzuki et al., 2009).

In the present study we focused on NADPH oxidase and tested whether its inhibitor, apocynin, might be able suppression of androgen-independent prostate cancer progression in vitro

* Corresponding author at: Nagoya City University Graduate School of Medical Sciences, 1 Kawasumi, Mizuho-cho, Mizuho-ku, Nagoya 467-8601, Japan.
Tel.: +81 52 853 8156; fax: +81 52 842 0817.
E-mail address: shugo@med.nagoya-cu.ac.jp (S. Suzuki).

0940-2993/$ – see front matter © 2013 Elsevier GmbH. All rights reserved.
http://dx.doi.org/10.1016/j.etp.2013.03.002